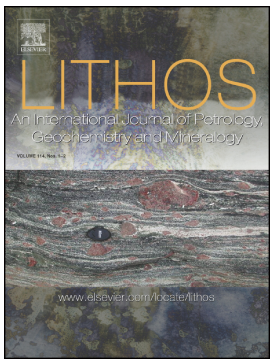

Contrasting noble gas compositions of peridotitic and eclogitic monocrystalline diamonds from the Argyle lamproite, Western Australia

S. Timmerman, M. Honda, X. Zhang, A.L. Jaques, G. Bulanova, C.B. Smith, A.D. Burnham

PII: S0024-4937(19)30267-1
DOI: https://doi.org/10.1016/j.lithos.2019.06.027
Reference: LITHOS 5125

To appear in: *LITHOS*

Received date: 11 January 2019
Accepted date: 22 June 2019

Please cite this article as: S. Timmerman, M. Honda, X. Zhang, et al., Contrasting noble gas compositions of peridotitic and eclogitic monocrystalline diamonds from the Argyle lamproite, Western Australia, LITHOS, https://doi.org/10.1016/j.lithos.2019.06.027

For Lithos

Contrasting noble gas compositions of peridotitic and eclogitic monocrystalline diamonds from the Argyle lamproite, Western Australia

S Timmerman[1*], M Honda[1], X Zhang[1], AL Jaques[1], G Bulanova[2], CB Smith[2], AD Burnham[1]

[1] *Research School of Earth Sciences, Australian National University, Acton ACT 2601, Australia.*

**Correspondence to suzette.timmerman@anu.edu.au*

[2] *School of Earth Sciences, University of Bristol, Bristol BS8 1RJ, United Kingdom*

Abstract

He-Ne-Ar compositions were determined in diamonds from the Argyle lamproite, Western Australia, to assess whether subducted material affects the noble gas budget and composition of stable old sub-continental lithospheric mantle (SCLM). Twenty diamonds (both peridotitic and eclogitic) were characterized for their carbon isotopic compositions and N abundance and aggregation from which 10 eclogitic growth zones and 5 peridotitic growth zones were analysed for their He-Ne-Ar compositions. The eclogitic diamonds have $\delta^{13}C$ values of -4.7 to -16.6‰ indicating a subduction signature, whereas the peridotitic diamonds have mantle-like compositions of -4.0 to -7.8‰. Mantle residence temperatures based on N-in-diamond thermometry showed that the eclogitic diamonds were mainly formed at 1260-1270°C or above 1300°C near the base of the lithosphere, whereas the peridotitic diamonds generally formed at lower temperatures (mostly 1135-1230°C). A noble gas subduction signature is present to various extents in the eclogitic diamonds and is inferred from a hyperbolic mixing relationship between R/Ra and ^4He and $\delta^{13}C$ values concentrations with a predominance of low R/Ra values (<0.5; $R/Ra = {}^3He/{}^4He_{sample} / {}^3He/{}^4He_{air}$). In addition, low $^{40}Ar/^4He$ and $^{40}Ar/^{36}Ar$ ratios, high nucleogenic $^{21}Ne/^4He$ and low $^3He/^{22}Ne$ ratios are characteristic of subducted material and were found in the eclogitic diamonds. The peridotitic diamonds show generally higher R/Ra values (median 1.1 ± 1.1) and lower $^4He/^{40}Ar$ ratios compared to eclogitic diamonds (median 0.1 ± 0.8 R/Ra; with 7/10 samples having an average of 0.13 ± 0.14 R/Ra). The studied peridotitic diamond growth zones showed a negative correlation between R/Ra and ^4He concentrations over 2 orders of magnitude and limited variation in ^3He, that can be largely explained by radiogenic ^4He ingrowth. At low ^4He concentrations the R/Ra value is

around 2.8 for both paragenesis of diamonds and is significantly lower than present-day SCLM values, suggesting (1) a more radiogenic helium isotope composition beneath the Halls Creek Orogen than those for typical SCLM from other cratons and/or (2) that the peridotitic diamonds are formed from fluids that also had a subduction input. The high mantle residence temperature and low R/Ra value in the core and low temperature and higher R/Ra value in the rim of a single peridotitic diamond indicate multiple growth events and that part of the lherzolitic diamond population may be genetically related to the eclogitic diamonds. Combining the diamond mantle residence temperatures with noble gas compositions shows that noble gas subduction signatures are present at the base of the lithosphere below 180 km depth beneath Argyle and that fluid migration and interaction with the SCLM occurred over scales of at least 15 kilometres, between 180 and 165 km depth.

Keywords: deep volatile cycles, lithospheric mantle, metasomatism, diamond growth, subduction

1 Introduction

Noble gases are volatile and incompatible in the Earth's mantle, and for these reasons very sensitive indicators of the source components, partial melting, melt migration and mixing processes in the mantle. The distinct noble gas signatures of the upper mantle and crustal/atmospheric sources enable them to be used to trace the influence of subducted crustal materials and subsequent homogenization with the mantle. Previous studies have shown that the heavy noble gases (Ne, Ar, Kr, Xe) are subducted into the mantle (Holland and Ballentine, 2006; Kendrick et al., 2011; Kendrick et al., 2018). Noble gases are incompatible in minerals relative to fluids (e.g. Heber et al., 2007) and hence are largely lost from their mineral hosts in the subducting slab during metamorphic dehydration reactions and melt formation. Lower temperatures suppress dehydration, melting and diffusion, and therefore subduction of noble gases is most efficient along cold subduction zones (Smye et al., 2017) where the noble gases are carried down in serpentinite and amphibole minerals (e.g. Kendrick et al., 2011; 2015; Tolstikhin et al., 2016). The amount and depth of noble gas subduction beyond depths associated with arc magma genesis is, however, not well constrained. Additionally, it is not known to what extent the subduction zones affect the noble gas budget and composition of stable old sub-continental lithospheric mantle (SCLM). Diamonds lock in

noble gases during their formation in the SCLM and subduction zones, and can therefore provide valuable information to resolve these issues.

Previous studies of noble gases in diamonds have been focused on fibrous and polycrystalline diamonds (e.g. Ozima and Zashu, 1983, Ozima et al., 1985; Honda et al., 1987; Burgess et al., 1998; Wada and Matsuda, 1998; Honda et al., 2004; Gautheron et al., 2005; Burgess et al., 2009; Honda et al., 2011; see review in Basu et al., 2013; Broadley et al., 2018; Timmerman et al., 2018), due to their abundant fluid inclusions and higher gas concentrations relative to monocrystalline or gem-quality diamonds. Polycrystalline diamonds are especially affected by loss of the light noble gases (Gautheron et al., 2005) and ingrowth of radiogenic noble gases, and are therefore not suitable for investigating subduction influences. Noble gas studies on monocrystalline diamonds of known paragenesis and location are, however, very scarce. McConville et al. (1991) studied composite (several different diamonds combined) monocrystalline diamonds of unknown paragenesis from the Argyle deposit, but these were affected by ^{4}He implantation from surrounding U-Th rich material in the case of diamonds mined from the pipe and cosmogenic ^{3}He for the alluvial diamonds, and therefore the helium results are not readily interpretable. Honda et al. (2012) determined noble gas compositions of three industrial-grade monocrystalline diamonds from Argyle of possible eclogitic paragenesis and proposed a subduction influence. Kurz et al. (1987) found the helium isotope data of two peridotitic and two eclogitic diamonds from Orapa to be indistinguishable, though some differences are clearly visible in the step-heating experiments of that study. As a result, a larger-scale study of the noble gas compositions of well-characterised diamonds is warranted. The Argyle diamond deposit was chosen for our research as it is ideal for such a study because of a distinction in residence temperatures between eclogitic and peridotitic diamonds, with eclogitic diamonds being indicated as formed at the base of the SCLM with a subduction influence and peridotitic diamonds formed mainly at shallower depths (Jaques et al., 1989a; Stachel et al., 2018).

In this study we present a combined carbon isotope and nitrogen content and aggregation state study along core to rim profiles of twenty Argyle diamonds to assess whether the diamonds were formed in single or multiple growth events. The samples are characterized by paragenesis based on mineral inclusions and carbon isotope compositions, and for their mantle residence temperatures based on nitrogen systematics. Subsequently He and Ar isotope analyses were performed on the major growth zones of 8 eclogitic and 3 peridotitic diamonds. The present study is the first systematic study to compare helium and argon isotope compositions of eclogitic and peridotitic monocrystalline diamonds collected from the same

kimberlite or lamproite pipe with the aim of evaluating the influence of subduction of noble gases on the sub-continental lithosphere noble gas composition.

2 Geological background

The major Argyle diamond deposit is hosted in the AK1 lamproite pipe, located in the Proterozoic Halls Creek orogenic belt at the margin of the Kimberley Craton in northwest Australia. The lamproite erupted around 1.18 Ga (1178 ± 47 Ma based on Rb-Sr phlogopite – whole rock isochron; Pigeon et al., 1989; Rayner et al., 2018) and ascended through a depleted Archean sub-continental lithospheric mantle (Luguet et al., 2009; Jaques et al., 2018). Argyle peridotite xenoliths have low FeO and Al_2O_3 contents that are evidence of a depleted mantle, and record equilibration temperatures and pressures of 1050-1330 °C and 4.8-6.1 GPa (equal to depths of 150-200 km; Jaques et al., 1990; Luguet et al., 2009; Jaques et al., 2018). Peridotitic silicate inclusions in Argyle diamonds have equilibration temperatures within this range (1120° to 1230°C at 5 GPa; Jaques et al., 1989a, 1994; Stachel et al., 2018) and the extent of nitrogen aggregation of peridotitic diamonds gives a mantle residence temperature of 1250 ± 60 °C. Trautman (1999) obtained similar mantle residence temperatures (1250-1300 ºC) for microdiamonds recovered from Argyle peridotite xenoliths. Rhenium-osmium dating indicates an Archean age for the peridotite xenoliths (Graham et al., 1999) with most having rhenium depletion model ages (T_{RD}) of 2.3-3.2 Ga (Luguet et al., 2009).

While eclogitic diamonds form the majority of the diamond population at Argyle (>90%), no eclogitic xenoliths have been recovered. Eclogitic silicate inclusions in Argyle diamonds show a wide range of compositions and equilibration temperatures of 1085-1350 °C (Jaques et al., 1989a; Stachel et al., 2018). High K_2O contents found in many omphacite inclusions indicate formation at high pressures of 6-6.5 GPa near the base of the lithosphere (Jaques et al., 1989a; Luguet et al., 2009). Stachel et al. (2018) reported 3 garnet inclusions (2 eclogitic, 1 peridotitic) with a small majorite component indicating formation at slightly higher pressures (up to ~8 GPa). Another Argyle eclogitic diamond with a two-phase garnet-omphacite inclusion was inferred to have re-equilibrated from former majorite garnet at an even higher formation pressure of 9 GPa, equivalent to ~300 km depth (Bulanova et al., 2018). Nitrogen aggregation in eclogitic diamonds indicates mantle residence temperatures of 1085-1366 °C (at a residence time of 0.4 Ga; Taylor et al., 1990; Viljoen, 2002), with the majority residing at 1250-1300 °C consistent with an origin near the base of the lithosphere (Bulanova et al., 2018; Stachel et al., 2018). Pooled eclogitic garnet and clinopyroxene inclusions yield a Sm-Nd age of 1580 ± 60 Ma (Richardson, 1986). As noted by Luguet et al. (2009) this age does not appear to be associated with significant geological events in the Halls Creek Orogen or elsewhere on

the Kimberley Craton but does coincide with major thermal and tectonic events involving crustal shortening that affected other terranes of the North Australian Craton (see for example Betts and Giles, 2006; Cawood and Korsch, 2008). Subduction at the Kimberley Craton margin is inferred to have occurred in the early Paleoproterozoic and was followed by collision and terrane accretion during the Hooper (1870–1850 Ma) and Halls Creek (1835–1805 Ma) orogenies that marked the collision and amalgamation of the Kimberley craton with the remainder of the North Australian craton (e.g., Griffin et al., 2000; Cawood and Korsch, 2008; Tyler et al., 2012). It has long been proposed that the eclogitic diamond population at Argyle was formed from subducted crustal carbon as the eclogitic diamonds have predominantly light C isotope compositions (-5 to -19 ‰, with most ~-11 to -12 ‰; Jaques et al., 1989a; Stachel et al., 2018). Other evidence for a subduction-related origin for the Argyle eclogitic diamonds are their noble gas compositions (low $^{40}Ar/^{36}Ar$, absence of $^{129}Xe/^{130}Xe$ anomalies; Honda et al. 2012), the association of heavy O isotope compositions in garnet and coesite (+6 to +16 ‰) with light carbon in the diamonds (Schulze et al., 2013), and positive Eu/Eu* anomalies and low Yb contents (attributed to plagioclase accumulation in mafic protoliths; Stachel et al., 2018) in eclogitic garnet inclusions from Argyle. For more information on major elements and trace elements of inclusions in Argyle diamonds, and on the geology of Argyle and the area, the reader is referred to Hall and Smith (1985), Griffin et al. (1988), Jaques et al. (1989a); Stachel et al. (2018), Rayner et al. (2018) and Jaques et al. (2018).

3 Materials and methods

3.1 Samples

Twenty diamonds from Argyle were studied for their internal structure by cathodoluminescence (CL), mineral inclusions by Raman spectroscopy and electron microprobe (EPMA), carbon isotope compositions by ion microprobe (SHRIMP-SI), and nitrogen systematics by Fourier transform infrared spectroscopy (FTIR). Subsequently, growth zones (n=15) were selected for further helium and argon isotope analyses, based on relatively homogeneous carbon isotope compositions of individual major growth zones and sufficient material available for noble gas measurements.

An overview of the studied samples is provided in Table 1 and Fig. A1. The first 12 sample numbers starting with ‘A’ are whole diamonds kindly provided by Argyle Diamond Mines Ltd. These samples were cut along the (110) crystallographic plane into a central plate (varying between 0.8 and 1.5 mm in thickness, except for A17 from the suite studied by Jaques et al., 1989a that was >2.5 mm) plus off cuts at Laseredge Services in Antwerp, and subsequently

polished at the Australian National University (ANU). The latter 8 samples with the prefix 'Arg' were off cuts or central plates provided by Argyle Diamonds Ltd for research by G. Bulanova and C.B. Smith. Central plates of samples Arg-36, Arg-26, Arg-006, Arg-41, Arg-89 were previously studied by Bulanova et al. (2018) by techniques indicated in Table 1. A detailed FTIR study of sample Arg-26 was previously undertaken by Kohn et al. (2016).

3.2 CL imaging, Raman and EPMA

Internal structures of the diamond central plates and off cuts were recorded by cathodoluminescence imaging, with a Robinson CL detector on a JEOL JSM-6610A scanning electron microscope at ANU. Inclusions were identified with Raman and EPMA. A coesite inclusion in Argyle sample A52 was identified with micro-Raman, where a laser with a wavelength of 532 nm was used on a Renishaw inVia™ confocal system at ANU. Exposed mineral inclusions were analysed for their major element composition (Table 2) on a Cameca SX100 Electron Probe Microanalyzer, with a beam current of 20 nA and an acceleration voltage of 15 kV, and on a JEOL 8530 FE EPMA with a beam current of 10 nA and an acceleration voltage of 15 kV. The elements on the Cameca were calibrated using the standards sanidine (Na, K), MgO (Mg), $CaAl_2O_4$ (Ca, Al), apatite (P), TiO_2 (Ti), Cr_2O_3 (Cr), rhodonite (Mn), SiO_2 (Si), Fe (Fe), and internally checked using San Carlos olivine and other international EPMA reference standards (augite, hornblende, and garnet; Jarosewich et al., 1980). The elements on the JEOL were calibrated using sanidine (Si, Al, K), diopside (Ca), chromite (Cr), rutile (Ti), apatite (P), periclase (Mg), rhodonite (Mn), and hematite (Fe), and checked with almandine garnet standards. Counts were transferred into concentrations using the X-Phi correction routine.

3.3 SHRIMP

Carbon isotope compositions were measured on *in-situ* spots (Table A1) with a 15 keV Cs^+ primary beam and a current of 13 nA on the Sensitive High Resolution Ion Microprobe – Stable Isotopes (SHRIMP-SI) at ANU. The SHRIMP-SI has a mass resolution of >5000 ($m/\Delta m$) and can therefore separate $^{13}C^-$ from $^{12}CH^-$ ions. For each analysis the background was measured in 6 scans of 20 seconds each, followed by optimizing the beam and data collection in 6 scans of 20 seconds each. The diamond standard MC08 was used as the primary calibration standard ($\delta^{13}C_{PDB}$ = −8.85 ± 0.19 ‰ (*n* = 37); standard from Stern et al., 2014). The stability of the instrument was monitored with an in-house nano-polycrystalline diamond (BS249; Irifune et al., 2003), which yielded $\delta^{13}C_{PDB}$ = −24.91 ± 0.32 ‰ (*n* = 70).

3.4 FTIR

Multiple spots were analysed for nitrogen content and aggregation state on core-rim traverses for each studied diamond (Table A2) on a Bruker Tensor 27 Hyperion FT-IR spectrometer attached to a Hyperion2000 microscope. This FTIR instrument has a 15x condenser lens, KBr beam splitter, and a liquid N_2 cooled MCT detector. Spectra were taken from 4000 to 650 cm^{-1} wavelength with a resolution of 2 cm^{-1} and a 50 µm spot size. The spectra were processed and deconvolved using DiaMap (Howell et al., 2012a, b), where each spectrum was fitted to a type IIa diamond spectrum in the two-phonon region by finding the minimum between 1990 and 1995 cm^{-1} wavelength and normalised to an absorption of 11.94 for 1 cm thickness. The nitrogen area was fitted with A, B, and D components and concentrations were calculated with conversion factors of 16.5 for A and 79.4 for B (Boyd et al., 1994; Boyd et al., 1995).

3.5 Noble gas mass spectrometry

Diamond fragments were cleaned at 120°C in concentrated HF, HNO_3, and 6 M HCl respectively over several nights, to remove any adherent material. After drying, weighing and wrapping in tin foil, the samples were loaded into a metal sample cursor that is connected to a high temperature double-vacuum tantalum furnace on-line to a high mass resolution (>1800) multi collector Helix-MC *Plus* noble gas mass spectrometer. The furnace section was subsequently baked at 150°C for 2 days and the Ta crucible was degassed for 5 hours each day for 5 days at 2000°C.

Details of the Helix-MC *Plus* set-up at ANU can be found in Zhang et al. (2016) and Zhang and Honda (2017). The general settings of the mass spectrometer were an acceleration voltage of 9.9 kV and source slit width of 0.1 mm. For the measurement of procedural hot blanks and diamond fragments the furnace was initially heated to 800 °C in dynamic operation to pump out gases released from surfaces of the diamond sample, tin wrapping, and crucible, and directly heated further to 2000 °C in static operation (60 min for heating to 2000 °C – settling 25 min at 2000 °C – 30 min for cooling) to release gases from the sample. The noble gases were purified by NP10 SAES getters and physically adsorbed to a Janis cryogenic charcoal system at 10 K and subsequently noble gases were released separately, starting with He at 40 K, followed by Ne at 115 K, and Ar at 250 K. A charcoal finger on-line to the mass spectrometer was held at liquid N_2 temperature to reduce isobaric interferences during He and Ne isotope analysis.

Helium data were collected in 20 cycles by peak jumping on the Faraday detector with a 10^{12} Ohm feedback resistor (^{4}He) and CDD detector (^{3}He) on the H1 collector, with a lower mass resolution of 1000. A calibrated small volume of neon was admitted into the mass

spectrometer to adjust the collector positions for H2 ($^{22}Ne^{+}$) and L2 ($^{20}Ne^{+}$). Subsequently the remaining volume fraction of neon was measured for 10 cycles in multi-collector mode. In a similar way argon data were collected for 20 cycles, with ^{40}Ar on the Faraday detector on H2, ^{38}Ar on the AX CDD and ^{36}Ar on the L2 CDD. Peak centering was done every 2 cycles for helium and neon, and every 4 cycles for argon.

3.6 Error propagation and blank contributions in noble gas analyses

Procedural hot blank levels at 2000 °C were <$9.7x10^{-12}$ ccSTP for ^{4}He, 1.5-$2x10^{-14}$ ccSTP for ^{3}He, 4.6-$5.3x10^{-12}$ ccSTP for ^{20}Ne, 2.7-$7.3x10^{-9}$ ccSTP for ^{40}Ar and 8.3-$22x10^{-12}$ ccSTP for ^{36}Ar. Blank contributions, relative to the total gas measured, were 0-0.5% for ^{4}He, 21-86% for ^{3}He (2 samples had no detectable ^{3}He above blank), and 30-80% for ^{40}Ar. The good reproducibility of the ^{3}He blank allows for reliable blank corrections. Argon results with a blank contribution of more than 80% for ^{40}Ar are excluded from Table 3. The argon blank decreased linearly over the 3 months of noble gas analyses and therefore a time-dependent blank correction was made (see the graphs in the Supplementary information A4 'noble gas raw data'). In the case of neon, only sample A50-1 had neon contents significantly above blank level with a 61% blank correction for ^{20}Ne (results described in section 4.4); neon results from all other samples had >88% blank correction and were discarded.

The data were corrected for CO_2^{++} interferences (in the case of Ne analyses), total procedural blank, sensitivity and mass discrimination (based on the HESJ standard for He; Matsuda et al., 2002 and a small Heavy Air gas standard for Ne and Ar), with fully propagated errors following error propagation laws. Details on the error propagation are provided in Appendix – Table A3.

4 Results

4.1 Diamond external and internal morphology

The samples in this study are colourless or brown (Fig. A1) with octahedral-dodecahedral morphologies. Diamond A56 was a macle. Most of the diamonds in the present study have frosting and trigonal or hexagonal pits. Cathodoluminescence images revealed that the internal structure of the peridotitic diamonds show clear tangential growth without significant distortion or evidence of stress (this study; Bulanova et al., 2018). Resorption of growth layers has occurred internally (Arg89) and externally (Arg41).

The CL images of the eclogitic diamonds are more complex (Fig. 1; Bulanova et al., 2018). While most eclogitic samples show tangential (layer-by-layer) growth, there are often distortion and elongations present (A50, A51, A52, A53, A56, A57, A60, Arg43; Fig. 1). These features are evidence of plastic deformation and thus a high stress environment. Distorted, rounded and unclear growth structures are present in A50, A51, A52, and A53. Internal resorption is also very common (A50, A51, A53, A56, A57, A58, Arg26, Arg36, A2-010). Several samples have multiple 'seeds' in the centre of the diamond, prior to growth layers around all the seedlings (A51, A53, A56, A57, A59). Cathodoluminescence images are given Figure 1, where the FTIR and SHRIMP-SI spot analyses locations are also indicated.

4.2 Paragenesis

The majority (~90%) of the diamonds recovered at the Argyle mine have an eclogitic paragenesis (Hall and Smith, 1985; Jaques et al., 1989a; Stachel et al., 2018). As this study is focused on comparing eclogitic and peridotitic diamonds, the sampling is biased with a deliberate over-representation of peridotitic diamonds. Division into the established peridotitic and eclogitic suites (e.g. Meyer, 1987) was based on the mineral inclusions found in the studied diamonds. Eclogitic garnet, eclogitic clinopyroxene or coesite were identified by Raman or EPMA analyses in 11 diamonds. The analysed pyrope-almandine garnet inclusions have compositions with low Cr_2O_3 contents (<0.1 wt%), a limited range in CaO contents (9.0-13.1 wt%), a large range in magnesium numbers (46-70; where Mg# = Mg/[Mg+Fe]*100), and belong to the eclogitic suite (Table 2). Diamond A17 also shows variation in the composition of included garnets (Table 2; Jaques et al., 1989a). Higher Na_2O and TiO_2 contents (up to 1.2 wt%; A54, A59) and a slight excess of Si are found in some of the garnets (A54) and indicate equilibration at higher temperatures and pressures (Bishop et al., 1978) in the sub-continental lithospheric mantle (<7 GPa). All these compositions fall within the compositional range of Argyle mineral inclusions previously recorded (Jaques et al., 1989a; Stachel et al., 2018). Olivine inclusions, belonging to the peridotitic suite, were identified in 3 diamonds and had magnesium numbers of 92-93 (Table 2 this study; Table 1 of Bulanova et al., 2018), but it is unknown whether they are harzburgitic or lherzolitic.

4.3 Carbon isotope compositions

Previous studies have shown that diamonds from Argyle have a distinct carbon isotope distribution with a range of -3.7 to -10.5‰ for peridotitic diamonds and -5 to -18.7‰ but with a

pronounced mode at -11 to -12‰ for eclogitic diamonds (Jaques et al., 1989a; Bulanova et al., 2018; Stachel et al., 2018). Peridotitic diamonds have been sub-divided into lherzolitic and harzburgitic paragenesis based on mineral inclusions and show some distinction in carbon isotope values of -10.5 to -4‰ and -7 to -4‰ respectively (Stachel et al., 2018). Based on the distinction in carbon isotope values, diamonds A53, A50, A55, and A58 are likely eclogitic considering their light carbon isotope values of -11.6, -12.3, -12.4 and -13.1‰ respectively (Table 1; Appendix Table A1). These carbon isotope compositions fall within the range of the previous studies, with individual analyses ranging from -4.0 to -7.8‰ for peridotitic and -4.7 to -16.6‰ for eclogitic diamonds. Intra-diamond carbon isotope variations are limited to <2‰ for 10 diamonds and 2-4‰ for the other 10 diamonds in this study (Appendix Table A1, Figure A2).

4.4 Nitrogen content and aggregation state

Our results of the diamond nitrogen content and aggregation state for individual spot analyses are given in Appendix Table A2 and Figure A2, with the minimum and maximum values for each sample provided in Table 1. All the studied diamonds have A-centres (pairs of nitrogen atoms) and/or B-centres (four nitrogen atoms around a vacancy), with the aggregation state expressed as %B (= 100*B / (A+B)). The eclogitic diamonds have contents of 15-888 at.ppm N and aggregation states of 46 to 100 %B (average 87 %B), whereas the peridotitic diamonds have 30-1439 at.ppm N (this study; Bulanova et al. 2018) and 15-100 %B (average 67 %B; Fig. 2). The generally higher N aggregation state of the eclogitic diamonds compared to peridotitic diamonds is consistent with previous FTIR studies of Argyle diamonds (Taylor et al., 1990; Viljoen, 2002; Bulanova et al., 2018; Stachel et al., 2018). As only spot analyses were conducted along core-to-rim traverses, it is likely that not all micro-heterogeneity was sampled, as is shown by the more limited variation found in this study for diamond Arg26 (73-80% IaB) compared to the variation found in the same diamond (58-98% IaB) by a more detailed study undertaken by Kohn et al. (2016). The N content and aggregation variation in individual diamonds presented in this study therefore records only larger scale perturbations, which is sufficient for the aim of our study.

4.5 Helium and argon isotope compositions

The helium and argon concentrations and isotope compositions of 15 major diamond growth zones from 11 of the diamonds studied are provided in Table 3. Based on the above defined

parageneses for the Argyle diamonds of this study, the noble gas systematics are described separately for peridotitic and eclogitic diamonds. The peridotitic diamonds have a limited variability in ^{3}He concentrations of 1.1-6.6 x 10^{-12} ccSTP/g (cm^3/g at standard temperature and pressure), and R/Ra values of 0.3-3.1 (Fig. 3a). In contrast, the eclogitic diamonds have an order of magnitude larger range in ^{3}He concentrations (0.2-53 x 10^{-13} ccSTP/g) and R/Ra values of <0.01 to 23.3 (Table 3). Both peridotitic and eclogitic diamonds in this study exhibit a correlation between R/Ra and ^{4}He (Fig. 3b), as was previously found in two eclogitic Orapa gem diamonds by Kurz et al. (1987).

The neon concentrations of most samples were at or below the total procedural blank and are therefore not shown or discussed. Only eclogitic diamond A50-1 had neon concentrations significantly above blank (7.9 x 10^{-12} ccSTP/g ^{22}Ne) and an isotopic composition of 12.45 ± 1.64 for ^{20}Ne/^{22}Ne and 0.0719 ± 0.0179 for ^{21}Ne/^{22}Ne (1SD), which may indicate a contribution of a nucleogenic Ne component slightly larger than those found in MORBs, though the isotopic compositions are within error of the air-MORB mixing line (Fig. 4; Sarda et al., 1988). The ^{40}Ar/^{36}Ar ratios are low for both peridotitic (258-5955) and eclogitic (243-765) diamonds. Some values are lower than the present-day atmospheric ^{40}Ar/^{36}Ar ratio of 298.6 (Lee et al., 2006) but are theoretically possible given that in the Archaean atmospheric argon compositions were lower (^{40}Ar/^{36}Ar of ~240-260 at 1.6 Ga, 167-211 at 3.0 Ga; Pujol et al. 2013). Argon ratios close to the atmospheric value have been found previously in Argyle gem diamonds (^{40}Ar/^{36}Ar = 301-1147; Honda et al., 2012; McConville et al., 1991).

5 Discussion

5.1 Variation in N systematics and δ^{13}C

Nitrogen aggregates in the diamond from single nitrogen atoms (C-centre) to pairs of nitrogen atoms (A-centre) to four nitrogen atoms around a vacancy (B-centre), and is dependent on time, temperature and nitrogen concentrations (Evans and Harris, 1989; Taylor et al., 1990). After about 200 Ma the nitrogen aggregation becomes relatively insensitive to time (Navon, 1999). Thus, nitrogen systematics are more useful as a thermometer than to constrain exact time differences between growth events. Mantle residence temperatures are calculated (Table A2) with the nitrogen aggregation thermometer (using values from Taylor et al., 1996) and platelet degradation thermometer (Speich et al., 2018). Isotherms and residence temperatures were determined with mantle residence times of 0.4 Gyr for eclogitic diamonds and 0.4 and 2.0 Gyr for peridotitic diamonds based on the difference between the lamproite eruption age (1.18 Ga; Pigeon et al., 1989) and diamond and xenolith formation ages (see section 2

Geological background). As multiple diamond-forming events occur in the mantle beneath other diamond mines (e.g. Pearson et al., 1998; Wiggers-de Vries et al., 2013; Timmerman et al., 2017), this is probably also the case in the mantle beneath Argyle. There is currently only limited diamond age data available for Argyle and for this reason we have calculated residence temperatures for both 0.4 and 2.0 Gyr residence times for peridotitic diamonds.

The studied peridotitic diamonds show mantle residence temperatures of 1231-1350, ~1135, and ~1200°C for samples Arg006, Arg41, Arg89, respectively, using the nitrogen aggregation thermometer and 2.0 Gyr residence time. Slightly higher temperatures (1277-1350, ~1175, and 1245°C) are calculated for these samples using a 0.4 Gyr residence time. Temperatures calculated with the platelet degradation thermometer are mostly comparable to temperatures of the nitrogen aggregation thermometer and within error (Table A2) using the uncertainties stated in Speich et al. (2018). The eclogitic diamonds, on the other hand, show residence temperatures of 1220-1360°C with most samples around 1260-1270 or above 1300°C. This confirms previous findings of mantle residence temperatures based on N of Argyle diamonds (Taylor et al., 1990; Viljoen, 2002; Bulanova et al., 2018; Stachel et al., 2018), with eclogitic diamonds formed mostly near the base of the lithosphere and at higher temperatures relative to most Argyle peridotitic diamonds, regardless of using a 0.4 or 2.0 Gyr residence time.

5.1.2 Intra diamond variations

Nitrogen concentrations vary widely within some of the studied diamonds, but generally decrease towards the rim (Fig. A2). Individual diamonds show a limited carbon isotopic variation internally (all <4‰ variation). There are limited systematic changes and coupling between N and $\delta^{13}C$ values. The observed large decreases in nitrogen content but insignificant changes in carbon isotope compositions within major growth zones can be caused by small amounts of Rayleigh fractionation processes, as was shown by Smart et al. (2011). Many of the studied diamonds do, however, show higher $\delta^{13}C$ values in their rims with respect to their cores (9/20 diamonds higher, 3/20 diamonds lower, 8/20 diamonds no significant difference with <0.4‰), possibly indicating that some of the fluids that formed the rims of these diamonds had interacted more extensively with mantle material causing a change towards more mantle-like $\delta^{13}C$ values. Further evidence for multiple diamond growth events comes from their changes in residence temperatures. The eclogitic diamonds A50 and A60 showed a range of temperature decreases from core to rim (1324 → 1262 °C and 1254 → 1220 °C respectively), indicating multiple growth events but from fluids with similar carbon isotope compositions. The temperature decreases from core to rim (>1340 → 1231 °C; Fig. 2) but similar $\delta^{13}C$ values in peridotitic diamond Arg-006 can be explained by the same process. The precision of the residence temperature calculated from N systematics is better than ±20°C in the case of Arg-

026 (Kohn et al., 2016) and is better for diamonds with higher nitrogen contents (> 100 at.ppm).

Core-rim traverses for N content, residence temperature, and $\delta^{13}C$ values of the Argyle diamonds studied are provided in the Appendix Fig. A2. While detailed evaluations of the N systematics and $\delta^{13}C$ values and assessment of likely Rayleigh fractionation and fluctuations in the nitrogen and carbon composition of the fluid are not the focus of this study, the N systematics and $\delta^{13}C$ values are important in assessing diamond growth and selection of growth zones appropriate in terms of homogeneity for noble gas analyses. It can be concluded from the variations identified that both the eclogitic and peridotitic diamond populations are formed in multiple growth events. This is important for the discussion below on ^{4}He ingrowth and comparing eclogitic and peridotitic diamonds. The N-$\delta^{13}C$ variation also shows more dating studies are needed to determine the number and timing of the various diamond growth events in the mantle beneath Argyle.

5.2 Differences in He-Ar between eclogitic and peridotitic diamonds

The ^{3}He concentrations of most peridotitic diamonds are higher than for eclogitic diamonds (Fig. 3a). The studied peridotitic diamonds have a similar range in ^{4}He concentrations to the eclogitic diamonds, but for a given ^{4}He concentration the R/Ra value (Fig. 3b) and ^{40}Ar concentration is equal to or higher than for those in the eclogitic diamonds. The range and difference in helium and argon concentrations and He isotopic compositions between peridotitic and eclogitic diamonds is not caused by ^{4}He implantation from neighbouring U-Th rich minerals (affecting the outer 27 µm of the diamond; Shelkov et al., 1998), as for all samples the outermost rim (30-50 µm) of the diamonds was removed. Cosmogenic ^{3}He production post-emplacement can also be discounted. All the diamonds studied were likely recovered from mining of the Argyle AK-1 pipe (rather than associated alluvial deposits that were mined up until 2003). The exception is sample A17 from the earlier study (Jaques et al., 1989a), which was recovered before 1985 and may have come from the alluvial deposits. The unusual high R/Ra of 23.3 and higher ^{3}He concentrations of this eclogitic sample A17-1 is therefore most likely the result of and can be explained by addition of a cosmogenic ^{3}He component formed by nuclear reactions with cosmic rays near the Earth's surface. Two models that may explain the difference in He-Ar between peridotitic and eclogitic diamonds

are (1) in-situ radiogenic ^{4}He ingrowth post-diamond formation and (2) formation of fluids with different chemical compositions. These two possibilities are evaluated below.

5.2.1 In-situ radiogenic ^{4}He ingrowth post-diamond formation

R/Ra values lower than those in the SCLM can be caused by in-situ radiogenic ^{4}He ingrowth after diamond formation. Estimations of the amount of radiogenic ^{4}He ingrowth since diamond formation can be made based on U and Th concentrations and the diamond and xenolith ages. For this evaluation we have used ages of 1600 Ma and 2200 Ma for eclogitic and peridotitic diamonds respectively. Upper limits are provided by the third quartile values (6.6 ppb Th and <LOQ U; maximum 1 ppb) of the 'dirtiest' (most inclusion-rich) Argyle monocrystalline diamonds measured with on-line LA-ICP-MS by Rege et al. (2010). This results in 4.8 x 10^{-7} ccSTP/g ^{4}He after 1600 Ma and 6.7 x 10^{-7} ccSTP/g ^{4}He after 2200 Ma. This corresponds to 11-74 % of the total ^{4}He for 11 samples and 100% for 4 samples of the measured concentrations. Median values of monocrystalline African and Canadian diamonds (0.20 ppb U) measured by off-line LA (Timmerman et al. 2019; Krebs et al., 2019) likely provide a more realistic estimate of U-Th concentrations we can expect in the Argyle diamonds in this study. Decay over 1600 (E-type) and 2200 (P-type) million years from these U-Th concentrations results in 9.16 x 10^{-8} ccSTP/g ^{4}He and 1.27 x 10^{-7},ccSTP/g ^{4}He respectively. This contributes 1.9-10% of the total observed ^{4}He for 7 of the 10 eclogitic diamond growth zones and 41.8-56.8% for the other 3 of the 10 eclogitic diamond growth zones. For peridotitic diamonds it makes up 2.1-5.8% (n=4) and 51.3% (n=1) of the total ^{4}He. This shows radiogenic ^{4}He ingrowth after diamond formation likely plays only a small role in three quarters of the samples but potentially a significant role in a quarter of the samples in the observed R/Ra value. The region where radiogenic ^{4}He ingrowth becomes significant for the eclogitic and peridotitic diamonds is shown in Figure 3c.

In R/Ra-^{4}He space the peridotitic diamonds and eclogitic diamonds both form trends (Fig. 3b), with lower R/Ra values present in samples with higher ^{4}He concentrations. As most eclogitic Argyle diamonds are likely formed in the same growth event, and the peridotitic diamonds are possibly related to each other, the role of radiogenic ^{4}He ingrowth can be evaluated further by modelling radiogenic ingrowth from a set initial R/Ra value and the median ^{3}He content. An initial R/Ra value of 4 was chosen, and ^{3}He contents of 5.6x10^{-13} and 4.1x10^{-12} ccSTP/g for the eclogitic and peridotitic diamonds respectively. The formula of Graham et al. (1987; ^{4}He* = 2.8x10^{-8} x 7.35 x U (ppm) x t (Myr)) was used for modelling the ingrowth, with a Th/U ratio of 3, 1600 Myr (E-type) and 2000 Myr (P-type) and varying U contents. While the modelled

curves (Fig. 3b) can reproduce most of the data, the amount of U (12 ppb for P-type, 15 ppb for E-type) needed to produce the lowest observed R/Ra values is an order of magnitude higher than the bulk of the literature range for gem-quality diamonds (<1.2 ppb U *n*=28, only one sample had 15 ppb; Timmerman et al., 2019; Krebs et al., 2019). In addition, the plotted modelled curves are R/Ra values versus the ingrowth of ^{4}He, which is shifted relative to curves of R/R values versus total ^{4}He (initial+ingrowth) and would result in a poor fit for the peridotitic diamonds. The appropriateness of radiogenic ingrowth curves for the Argyle samples can be assessed using R/Ra values versus the reciprocal of the helium concentration. Mixing trends are hyperbolic in R/Ra vs [He] and linear in R/Ra vs 1/[He] space, whereas radiogenic decay trends are curved in R/Ra vs [He] and remain curved in R/Ra vs 1/[He]. Figure 3d shows that a mixing line shows a better fit than the radiogenic growth curve for the eclogitic diamonds, particularly at lower helium concentrations (higher 1/[He]), and thus a mixing process is involved in the fluids that form the eclogitic Argyle diamonds.

However, the peridotitic Argyle diamonds show a negative correlation between R/Ra and ^{4}He concentrations over 2 orders of magnitude and only less than 1 order of magnitude variation in ^{3}He (Fig. 3a), suggesting this could largely be caused by radiogenic ingrowth. The lower R/Ra values of the cores of peridotitic diamonds Arg-006 (0.3 R/Ra) and Arg-41 (1.1 R/Ra) relative to their rims (1.8 and 3.1 R/Ra, respectively), might indicate older cores that had more time for radiogenic ^{4}He ingrowth. Nitrogen systematics of diamond Arg-006 indicates an age gap between core and rim, so the additional ^{4}He in the core could potentially be accounted for by greater radiogenic ingrowth. Arg-41 shows no age gap between core and rim and therefore the higher R/Ra of the rim must be due to a lower (U+Th)/^{3}He ratio of the diamond forming fluid, a change that may coincide with the decrease in N concentration (Table A2).

5.2.2 Different fluid compositions for formation of peridotitic and eclogitic diamonds

As mixing may be involved, we evaluate what sources are likely involved, based on the chemical evidence from this and previous studies. The distinction in fluid compositions between the peridotitic and eclogitic diamonds is evident in plots of R/Ra values versus helium concentrations (Fig. 3a, b), R/Ra versus δ^{13}C values (Fig. 5), and in R/Ra values (Fig. 6a) and ^{4}He/^{40}Ar ratios (Fig. 6b), and suggests at least two different sources. Peridotitic diamonds have carbon isotope compositions indicative of primarily mantle-sourced carbon (Jaques et al., 1989a; Stachel et al., 2018; this study). While there is significant overlap in R/Ra values, the peridotitic diamonds with heavier carbon isotope compositions show generally higher R/Ra values (median 1.1 ± 1.1; Fig. 6a) compared to eclogitic diamonds (median 0.1 ± 0.8, excluding sample A17-1), which have lighter carbon isotope compositions. R/Ra values at low ^{4}He

concentrations are ~2.8 and approaches the proposed present-day SCLM He composition of 5.9±1.2 R/Ra (Day et al., 2005). The peridotitic diamonds show $^{4}He/^{40}Ar$ ratios close to fibrous diamonds (Fig. 6b) with an SCLM-like He-Ar composition (Panda, Jwaneng; Burgess et al., 1998; 2009). This argues for a large mantle/SCLM component in the source of peridotitic diamond-forming fluids.

Eclogitic diamonds, on the other hand, have a large enrichment in ^{4}He relative to ^{40}Ar, compared to a mantle $^{4}He/^{40}Ar$ ratio of 1.4-4.8 (Matsuda and Marty, 1995). This may be explained by involvement of subducted material that is enriched in U and Th and has low K/U ratios relative to the mantle. However, the difference in K/U ratios of upper continental crust (9475; Rudnick and Gao, 2014) (that will be weathered, eroded, and subducted) and MORB (16775; White and Klein, 2014) is only a factor of 2, whereas the difference between the average eclogitic and peridotitic $^{40}Ar/^{4}He$ ratio is a factor of ~5. This poses the question whether potassium can be lost relative to uranium during subduction and cause the systematic difference in absolute ^{40}Ar concentrations between eclogitic and peridotitic diamonds (Table 3). Further evidence for the involvement of subducted material in eclogitic diamond-forming fluids is provided by He/Ne ratios of the studied diamonds.

The ^{3}He/solar ^{22}Ne ratio of 0.034 ± 0.027 (1SD) calculated for diamond A50-1 is significantly lower than the solar (~1.5; Tucker and Mukhopadhyay, 2014) and mantle values (~10; Tucker and Mukhopadhyay, 2014), suggesting ^{3}He was lost relative to solar ^{22}Ne. Nucleogenic ^{21}Ne is mainly produced via the reaction $^{18}O(\alpha,n)^{21}Ne$, with α particles generated by U-Th decay. Any radiogenic ^{4}He produced in the mantle and in fluid inclusions in diamonds (initial trapped ^{4}He + in-situ radiogenic ^{4}He), where oxygen is present, should thus be accompanied by nucleogenic ^{21}Ne. Sample A50-1 has a ^{22}Ne concentration of 7.9×10^{-12} ccSTP/g and a $^{21}Ne/^{22}Ne$ ratio of 0.0719 ± 0.0179 (1SD). Solving the mixing equations of air, solar, and nucleogenic neon, the sample contains a nucleogenic component of 3.2×10^{-13} ccSTP/g ^{21}Ne and a nucleogenic $^{21}Ne/^{4}He$ ratio of 1.44×10^{-7}. This is higher than the nucleogenic $^{21}Ne^{*}$/radiogenic $^{4}He^{*}$ production ratio of the Earth's mantle (4.56×10^{-8}; Yatsevich and Honda, 1997) and indicates ^{4}He, originally residing in the crust/sediments, was lost relative to ^{21}Ne, most likely during subduction. The discrepancy in depletion factors between $^{3}He/^{22}Ne$ (0.0034) and $^{4}He/^{21}Ne$ ratios (0.32) relative to the solar and radiogenic/nucleogenic production ratios further indicates that the original He (^{3}He and ^{4}He) in the slab has been totally lost but the majority of $^{4}He^{*}$ produced in the slab during subduction reaches and is present in the diamond-forming regions. In addition, radiogenic ^{4}He is produced within the diamond.

A subduction component is further supported by low $^{40}Ar/^{36}Ar$ compositions (this study; Honda et al., 2012) and noble gas abundance patterns found in 3 diamonds from Argyle (Honda et al., 2012). Eclogitic diamonds from Argyle and Orapa (this study; Kurz et al., 1987; Honda et al., 2012) have a greater abundance of low R/Ra values compared to peridotitic diamonds (Fig. 6a). This is consistent with the presence of a subduction component, as Gautheron and Moreira (2002) proposed that mixing of He is inefficient in the SCLM and mixing with subducted material results in more sampling of low R/Ra values. Low R/Ra values found in the eclogitic diamonds in this study are also consistent with low R/Ra values found in eclogitic xenoliths associated with subduction (Day et al., 2015).

The two sources that are likely involved in eclogitic diamond-forming fluids are subducted material and typical SCLM/mantle material. To evaluate if mixing between these two end-members is consistent with the observed variation in R/Ra-^{4}He and R/Ra-$\delta^{13}C$, mixing lines are calculated. The SCLM component is represented by a $\delta^{13}C$ value of -5‰ (Cartigny, 2005) and an R/Ra value of 26.6 (before in-situ radiogenic ingrowth at 1600 Ma; Seta et al., 2001) and an R/Ra value of ~4 after radiogenic ingrowth. The subduction component is set at a $\delta^{13}C$ value of -25‰ (close to the lowest value of altered oceanic crust that dominates the carbon budget; Li et al., 2019), and an R/Ra value of 0.005 (Ballentine and Burnard, 2002). The mixing between mantle and subduction component using $1x10^{-7}$ and $6x10^{-6}$ ccSTP/g ^{4}He respectively, can reproduce the observed R/Ra and ^{4}He values with 2SD of the eclogitic diamonds (Fig. 3b, d). Mixing between mantle and subduction components can explain the observed R/Ra and $\delta^{13}C$ values with high r values ($He/C_{subduction}$ / He/C_{mantle} ratios). Helium resident in a slab is likely (almost completely) lost during dehydration during subduction, resulting in a low ^{3}He abundance (Staudacher and Allegre, 1988), but some ^{4}He may be present due to radiogenic ingrowth from U-Th decay in the slab during the time between subduction and diamond formation. This was also observed in eclogitic xenoliths from South Africa, Siberia, and Morocco (Day et al., 2015). However, due to the extreme incompatibility of He, fluids coming off the slab have relatively high helium concentrations. This can result in high $He/C_{subduction}$ / He/C_{mantle} ratios. Mixing lines were also calculated at present-day, accommodating for 1600 Ma of radiogenic ^{4}He ingrowth from various U concentrations (Fig. 5). This shows that the observed R/Ra values in peridotitic diamonds are likely the result of radiogenic ^{4}He ingrowth and little or no subduction influence is required. Eclogitic diamonds, in contrast, are the result of both a subduction influence and subsequent in-situ radiogenic ^{4}He ingrowth.

5.3 Lherzolitic diamond growth and the helium composition of the SCLM beneath Argyle

When the correlation between R/Ra and ^{4}He of peridotitic diamonds is extrapolated to low ^{4}He concentrations (low in-situ produced radiogenic ^{4}He; Fig. 3b, d), the initial R/Ra value can be calculated and is representative of the starting composition/SCLM value beneath Argyle. This gives an R/Ra value of 2.8 at present-day, which is significantly lower than present-day CLM values for North America and Africa (5.9±1.2 R/Ra; Day et al., 2005). This suggests that the SCLM beneath the Halls Creek Orogen has a more radiogenic helium isotope composition than typical SCLM from other cratons and/or that at least some of the Argyle peridotitic diamonds were formed from fluids that had a subduction influence.

The peridotitic diamonds fall on the higher end of the 'mixing + radiogenic ^{4}He ingrowth' lines (Fig. 5), indicating that if there is a subduction influence, it only played a small or no role in the Argyle peridotitic diamond population. Evidence for a potential small subduction influence comes from peridotitic diamond Arg-006. The ^{3}He concentration of the core of this diamond is lower than of the rim, whereas the ^{4}He concentration is higher. This combination may suggest a subduction influence in the fluid that formed the core. The possibility of a lherzolitic diamond-forming event associated with subduction is supported by chemical evidence from previous studies; i) a distinct tail to lighter carbon isotope compositions of lherzolitic Argyle diamonds down to -10.5‰ caused by slab-derived fluids migrating into originally depleted peridotite (Stachel et al., 2018), and ii) enriched incompatible elements of peridotitic pyroxene inclusions in Argyle diamonds (Stachel et al., 2018) and xenoliths (Jaques et al., 2018). Further, the Argyle lamproite is enriched, which is inferred to have been derived by small degrees of melting of formerly depleted mantle that had undergone long-term geochemical enrichment (Jaques et al., 1989b; 2018).

The most likely scenario is that some of the peridotitic diamonds, namely the harzburgitic diamonds, were formed before the Paleoproterozoic subduction event with low R/Ra values caused by radiogenic ^{4}He ingrowth. However, part of the peridotitic diamond population - the lherzolitic diamonds - may be genetically related to the eclogitic diamonds with R/Ra-δ^{13}C - ^{4}He/^{40}Ar trends caused by mixing between subducted and mantle material through fluid migration and wall-rock interaction.

5.4 Percolation of subduction fluids into the SCLM

If the lherzolitic diamond population was formed after the Paleoproterozoic subduction and related to the eclogitic diamond growth event (Stachel et al., 2018), inferences can be made about scales and extents of fluid migration and interaction with the mantle. By combining mantle residence temperatures and noble gas compositions, a depth profile can be established by projection onto the paleogeotherm obtained from geothermobarometry of chrome diopsides xenocrysts recovered from the Argyle lamproite (Jaques et al., 2018). The mantle residence temperatures are comparable to formation temperatures (1085-1350 °C) based on geothermobarometry of garnet-clinopyroxene inclusions in Argyle eclogitic diamonds (Jaques et al., 1989a; Stachel et al., 2018). Nitrogen residence temperatures can therefore be used as a good approximation of the diamond formation temperature and thus depth of the diamond formation in the case of Argyle. Geothermobarometry data of Argyle diamond peridotitic mineral inclusions in previous studies are limited but generally confirm lower formation temperatures relative to those of eclogitic diamonds (Stachel et al., 2018). The eclogitic diamonds studied for noble gases here had temperatures that equate to 170-191 km depth, whereas the peridotitic diamonds resided at depths of 155-172 km (and the core of Arg-006 at 188 km) depth.

From the R/Ra and $^{40}Ar/^{4}He$ versus temperature graphs (Fig. 7a and b) it can be seen that at higher temperatures near the base of the lithosphere a clear subduction signature is present, whereas at lower temperatures (shallower depths) there is more variation in $^{3}He/^{4}He$ and $^{40}Ar/^{4}He$ ratios, with noble gas signatures trending towards mantle compositions. A similar trend is also visible in carbon isotope values, with lower $\delta^{13}C$ values at higher temperatures and more mantle-like $\delta^{13}C$ values at lower temperatures (Fig. 7c). When the temperatures are translated to a depth profile it shows subduction signatures are consistently present between 180 and 190 km depth, whereas various intensities of subduction signatures are present between 165 and 180 km (Fig. 8). This suggests that accreted subducted material is located at the base of the lithosphere and local heterogeneities caused by migration of subduction fluids extends over at least 15 kilometres. The percolation of subduction fluids into the SCLM is depicted in Figure 7d.

6 Conclusions

This study, based on twenty diamonds from Argyle, found abrupt changes in N-$\delta^{13}C$ across growth zones and a change in mantle residence temperature in one peridotitic and two eclogitic diamonds, indicating that not all diamonds were formed in one event and multiple diamond growth events occurred in the mantle beneath the Argyle deposit.

The strong plastic deformation and high mantle residence temperatures indicated by high levels of nitrogen aggregation of many of our studied eclogitic diamonds are consistent with the results of previous studies that indicate these diamonds formed in eclogitic source rocks accreted at the base of the lithosphere. Coupled with the 1.58 Ga age for Argyle eclogitic diamonds (Richardson, 1986) and the location of the Argyle pipe in the Paleoproterozoic orogenic belt at the craton margin, the major eclogitic diamond-forming event is linked to a Paleoproterozoic subduction event. Distinct differences in carbon isotope compositions between peridotitic (-4.0 to -7.8‰) and eclogitic (-4.7 to -16.6‰) Argyle diamonds further confirm the subduction signature in eclogitic diamonds and SCLM/mantle-like signature in peridotitic diamonds. The studied eclogitic Argyle diamonds have clear noble gas subduction signatures; a high abundance of low R/Ra values, a hyperbolic mixing relationship between R/Ra and ^{4}He and $\delta^{13}C$ values, low $^{40}Ar/^{4}He$ ratios indicating an enriched ^{4}He end-member consistent with ^{4}He ingrowth in subducted material, and a high nucleogenic $^{21}Ne/^{4}He$ and low $^{3}He/^{22}Ne$ ratio consistent with He being lost relative to Ne during subduction.

In contrast, the peridotitic diamonds show generally higher R/Ra values (median 1.1 ± 1.1) and higher $^{40}Ar/^{4}He$ ratios, compared to eclogitic diamonds (median 0.1 ± 0.8 R/Ra, excluding sample A17-1). The studied peridotitic diamond growth zones showed a negative linear correlation between R/Ra and ^{4}He concentrations over 2 orders of magnitude and only limited variation in ^{3}He, indicating this may be caused by radiogenic ingrowth of ^{4}He. Based on U concentrations from the literature, the in-situ radiogenic ^{4}He ingrowth in diamond since diamond formation is, however, not the only component contributing to the total ^{4}He concentrations observed in the samples. Projection of the noble gas trend in peridotitic diamonds towards extremely low ^{4}He concentrations (no significant in-situ radiogenic ^{4}He ingrowth) results in a R/Ra value of around 2.8, significantly lower than present-day SCLM values (5.9±1.2 R/Ra; Day et al., 2005), suggesting radiogenic ^{4}He ingrowth may have occurred prior to diamond formation. It also shows that the SCLM beneath the Halls Creek Orogen has a more radiogenic helium isotope composition than typical SCLM from other cratons and/or that these peridotitic diamonds are formed from fluids that also had a subduction influence. Based on the high mantle residence temperature in the core of peridotitic diamond Arg006 and its low R/Ra, we suggest that part of the peridotitic diamond population (the lherzolitic diamonds) may potentially be genetically related to the eclogitic diamonds. Other peridotitic (harzburgitic) diamonds likely formed before the subduction event (2.3-3.2 Ga Re-Os T_{RD} ages for peridotitic xenoliths; Luguet et al., 2009) from fluids of more SCLM-like composition. The R/Ra-$\delta^{13}C$ and R/Ra-$^{4}He/^{40}Ar$ of eclogitic diamonds can be generated by mixing between subducted and mantle material through fluid migration and wall-rock

interaction, plus in-situ radiogenic ^{4}He ingrowth. A depth profile shows noble gas subduction signatures are present at the base of the lithosphere up to 180 km depth and fluid migration and interaction with the SCLM towards higher R/Ra values occurs over scales of at least 15 km (to 165 km depth).

Acknowledgements

This research was supported by AGRTP and Ringwood scholarships to ST and funded by an ARC grant (DP140101976) to MH and ALJ. We thank John Chapman and Argyle Diamond Mines Ltd for providing the diamond samples. Robert Rapp and Jeff Chen are thanked for assistance with the EPMA analyses. The authors acknowledge the facilities, and the scientific and technical assistance, of Microscopy Australia at the Centre for Advanced Microscopy, The Australian National University. We also thank Sami Mikhail and anonymous reviewers for their constructive comments and suggestions that improved the presentation of this paper.

References

Ballentine, C.J., Burnard, P.G., 2002. Production, release and transport of noble gases in the continental crust. Reviews in mineralogy and geochemistry 47(1), 481-538.

Basu, S., Jones, A.P., Verchovsky, A.B., Kelley, S. P., Stuart, F.M., 2013. An overview of noble gas (He, Ne, Ar, Xe) contents and isotope signals in terrestrial diamond. Earth-science reviews 126, 235-249.

Betts, P.G., Giles, D., 2006. The 1800–1100 Ma tectonic evolution of Australia. Precambrian Research 144(1-2), 92-125.

Bishop, F.C., Smith, J.V., Dawson, J.B., 1978. Na, K, P and Ti in garnet, pyroxene and olivine from peridotite and eclogite xenoliths from African kimberlites. Lithos 11, 155-173.

Boyd, S.R., Kiflawi, I., Woods, G.S., 1994. The relationship between infrared absorption and the A defect concentration in diamond. Philosophical Magazine B 69(6), 1149-1153.

Boyd, S.R., Kiflawi, I., Woods, G.S., 1995. Infrared absorption by the B nitrogen aggregate in diamond. Philosophical Magazine B 72(3), 351-361.

Broadley, M.B., Kagi, H., Burgess, R., Zedgenizov, D., Mikhail, S., Almayrac, M., Ragozin, A., Pomazansky, B., Sumino, H., 2018. Plume-lithosphere interaction and the formation of fibrous diamonds. Geochemical Perspectives Letters 8, 26-30.

Bulanova, G.P., Speich, L., Smith, C.B., Gaillou, E., Kohn, S.C., Wibberley, E., Chapman, J.G., Howell, D., Davy, A.T., 2018. The unique nature of Argyle fancy diamonds. Internal structure, paragenesis, and reasons for color. Society of Economic Geologists, Special Publication 20, 169–190.

Burgess, R., Johnson, L.H., Mattey, D.P., Harris, J.W., Turner, G., 1998. He, Ar and C isotopes in coated and polycrystalline diamonds. Chemical Geology 146(3-4), 205-217.

Burgess, R., Cartigny, P., Harrison, D., Hobson, E., Harris, J.W., 2009. Volatile composition of microinclusions in diamonds from the Panda kimberlite, Canada: Implications for chemical and isotopic heterogeneity in the mantle. Geochimica et Cosmochimica Acta 73(6), 1779-1794.

Cartigny, P., 2005. Stable isotopes and the origin of diamond. Elements 1(2), 79-84.

Cawood, P.A., Korsch, R.J., 2008. Assembling Australia: Proterozoic building of a continent. Precambrian Research 166(1-4), 1-35.

Day, J.M., Hilton, D.R., Pearson, D.G., Macpherson, C.G., Kjarsgaard, B.A., Janney, P.E., 2005. Absence of a high time-integrated 3He/(U+Th) source in the mantle beneath continents. Geology 33(9), 733-736.

Day, J. M., Barry, P. H., Hilton, D. R., Burgess, R., Pearson, D. G., & Taylor, L. A., 2015. The helium flux from the continents and ubiquity of low-$^{3}He/^{4}He$ recycled crust and lithosphere. Geochimica et Cosmochimica Acta, 153, 116-133.

Evans, T., Harris, J.W., 1989. Nitrogen aggregation, inclusion equilibration temperatures and the age of diamonds. Ross J., et al. (Eds.), Kimberlites and Related Rocks, Vol. 2, Blackwell (1989), pp. 1001-1006

Gautheron, C., Moreira, M., 2002. Helium signature of the subcontinental lithospheric mantle. Earth and Planetary Science Letters 199(1-2), 39-47.

Gautheron, C., Cartigny, P., Moreira, M., Harris, J.W., Allegre, C.J., 2005. Evidence for a mantle component shown by rare gases, C and N isotopes in polycrystalline diamonds from Orapa (Botswana). Earth and Planetary Science Letters 240(3), 559-572.

Graham, D.W., Jenkins, W.J., Kurz, M.D., Batiza, R., 1987. Helium isotope disequilibrium and geochronology of glassy submarine basalts. Nature, 326(6111), 384-386.

Graham, S., Lambert, D.D., Shee, S.R., Smith, C.B., Reeves, S., 1999. Re-Os isotopic evidence for Archean lithospheric mantle beneath the Kimberley block, Western Australia. Geology 27(5), 431-434.

Graham, D.W., 2002. Noble gas isotope geochemistry of mid-ocean ridge and ocean island basalts: Characterization of mantle source reservoirs. Reviews in mineralogy and geochemistry 47, 247-317.

Griffin, T.J., Page, R.W., Sheppard, S., Tyler, I.M., 2000. Tectonic implications of Paleoproterozoic post-collisional high-K felsic igneous rocks from the Kimberley region of Northwestern Australia. Precambrian Research 101, 1-13.

Griffin, W.L., Jaques, A.L., Cousens, D., Ryan, C., Sie, S., Suter, G., 1988. Conditions of diamond growth: a proton microprobe study of inclusions in West Australian diamonds: Contributions to Mineralogy and Petrology 99, 143-158.

Hall, A.E., Smith, C.B., 1985. Lamproite diamonds—are they different? in Glover, J.E, and Harris, P.G., eds., Kimberlite occurrence and origin: A basis for conceptual models in exploration. Perth, Geology Department and University Extension, University of Western Australia, Publication No. 8, 167–212.

Heber, V.S., Brooker, R.A., Kelley, S.P., Wood, B.J., 2007. Crystal–melt partitioning of noble gases (helium, neon, argon, krypton, and xenon) for olivine and clinopyroxene. Geochimica et Cosmochimica Acta 71(4), 1041-1061.

Holland, G., Ballentine, C.J., 2006. Seawater subduction controls the heavy noble gas composition of the mantle. Nature 441(7090), 186-191.

Honda, M., Reynolds, J.H., Roedder, E., Epstein, S., 1987. Noble gases in diamonds: Occurrences of solarlike helium and neon. Journal of Geophysical Research: Solid Earth 92(B12), 12507-12521.

Honda, M., Phillips, D., Harris, J.W., Yatsevich, I., 2004. Unusual noble gas compositions in polycrystalline diamonds: preliminary results from the Jwaneng kimberlite, Botswana. Chemical Geology 203(3), 347-358.

Honda, M., Phillips, D., Harris, J.W., Matsumoto, T., 2011. He, Ne and Ar in peridotitic and eclogitic paragenesis diamonds from the Jwaneng kimberlite, Botswana—Implications for mantle evolution and diamond formation ages. Earth and Planetary Science Letters 301(1), 43-51.

Honda, M., Phillips, D., Kendrick, M.A., Gagan, M.K., Taylor, W.R., 2012. Noble gas and carbon isotope ratios in Argyle diamonds, Western Australia: Evidence for a deeply subducted volatile component. Australian Journal of Earth Sciences 59(8), 1135-1142.

Howell, D., O'Neill, C.J., Grant, K.J., Griffin, W.L., Pearson, N.J., O'Reilly, S.Y., 2012a. μ-FTIR mapping: distribution of impurities in different types of diamond growth. Diamond and Related Materials 29, 29-36.

Howell, D., O'Neill, C.J., Grant, K.J., Griffin, W.L., O'Reilly, S.Y., Pearson, N.J., Stern, R.A., Stachel, T., 2012b. Platelet development in cuboid diamonds: insights from micro-FTIR mapping. Contributions to Mineralogy and Petrology 164(6), 1011-1025.

Irifune, T., Kurio, A., Sakamoto, S., Inoue, T., Sumiya, H., 2003. Materials: Ultrahard polycrystalline diamond from graphite. Nature 421, 599-600.

Jaques, A. L., Sheraton, J. W., Hall, A. E., Smith, C. B., Sun, S. S., & Drew, R., 1989a. Composition of crystalline inclusions and C-isotopic composition of Argyle and Ellendale diamonds. In J. Ross, et al. (Eds.), Kimberlites and Related Rocks, Their Crust/Mantle Setting, Diamonds and Diamond Exploration. Geological Society of Australia Special Publication No14, vol. 2, 966-989.

Jaques, A. L., Sun, S.-S., Chappell, B.W., 1989b. Geochemistry of the Argyle (AK1) lamproite pipe, Western Australia, In J. Ross, et al. (Eds.), Kimberlites and Related Rocks, Their Composition, Occurrence, Origin and Emplacement. Geological Society of Australia Special Publication No14, vol. 1, 170-188.

Jaques, A. L., O'Neill, H. S. C., Smith, C. B., Moon, J., & Chappell, B. W. (1990). Diamondiferous peridotite xenoliths from the Argyle (AK1) lamproite pipe, Western Australia. Contributions to Mineralogy and Petrology 104(3), 255-276.

Jaques, A.L., Luguet, A., Smith, C.B., Pearson, D.G., Yaxley, G.M., Kobussen, A.F., 2018. Nature of the mantle beneath the Argyle AK1 lamproite pipe: constraints from mantle xenoliths, diamonds, and lamproite geochemistry. Society of Economic Geologists, Special Publication 20, 119–143.

Jarosewich, E., Nelen, J.A., Norberg, J.A., 1980. Reference samples for electron microprobe analysis. Geostandard Newsletter 4, 43–47.

Kendrick, M.A., Scambelluri, M., Honda, M., Phillips, D., 2011. High abundances of noble gas and chlorine delivered to the mantle by serpentinite subduction. Nature Geoscience, 4(11), 807-812.

Kendrick, M.A., Honda, M., Vanko, D.A., 2015. Halogens and noble gases in Mathematician Ridge meta-gabbros, NE Pacific: implications for oceanic hydrothermal root zones and global volatile cycles. Contributions to Mineralogy and Petrology 170(5-6), 43, 1-20.

Kendrick, M.A., Scambelluri, M., Hermann, J., Padrón-Navarta, J.A., 2018. Halogens and noble gases in serpentinites and secondary peridotites: Implications for seawater subduction and the origin of mantle neon. Geochimica et Cosmochimica Acta, 235, 285-304.

Kennedy, C.S., Kennedy, G.C., 1976. The equilibrium boundary between graphite and diamond. Journal of Geophysical Research, Solid Earth and Planets, 81, 2467-2470.

Kohn, S.C., Speich, L., Smith, C.B., Bulanova, G.P., 2016. FTIR thermochronometry of natural diamonds: A closer look. Lithos, 265, 148-158.

M.Y. Krebs, D.G. Pearson, T. Stachel, F. Laiginhas, S. Woodland, I. Chinn, J. Kong, 2019. A common parentage-low abundance trace element data of gem diamonds reveals similar fluids to fibrous diamonds. Lithos 324–325, 356-370.

Kurz, M.D., Gurney, J.J., Jenkins, W.J., Lott III, D.E., 1987. Helium isotopic variability within single diamonds from the Orapa kimberlite pipe. Earth and planetary science letters 86(1), 57-68.

Lee, J.Y., Marti, K., Severinghaus, J.P., Kawamura, K., Yoo, H.S., Lee, J.B., Kim, J.S., 2006. A redetermination of the isotopic abundances of atmospheric Ar. Geochimica et Cosmochimica Acta, 70(17), 4507-4512.

Li, K., Li, L., Pearson, D.G., Stachel, T., 2019. Diamond isotope compositions indicate altered igneous oceanic crust dominates deep carbon recycling. Earth and Planetary Science Letters, 516, 190-201.

Luguet, A., Jaques, A.L., Pearson, D.G., Smith, C.B., Bulanova, G.P., Roffey, S.L., Rayner, M.J. Lorand, J.P., 2009. An integrated petrological, geochemical and Re–Os isotope study of peridotite xenoliths from the Argyle lamproite, Western Australia and implications for cratonic diamond occurrences. Lithos 112, 1096-1108.

Mather, K., Pearson, D.G., McKenzie, D., Kjarsgaard, B.A., Priestley, K., 2011. Constraints on the depth and thermal history of cratonic lithosphere from peridotite xenoliths, xenocrysts and seismology. Lithos 125, 729–742.

Matsuda, J.I., Marty, B., 1995. The $^{40}Ar/^{36}Ar$ ratio of the undepleted mantle; a re-evaluation. Geophysical research letters 22(15), 1937-1940.

Matsuda, J., Matsumoto, T., Sumino, H., Nagao, K., Yamamoto, J., Miura, Y., Kaneoka, I., Takahata, N., Sano, Y., 2002. The 3He/4He ratio of the new internal He Standard of Japan (HESJ). Geochemical Journal 36(2), 191-195.

Mattey, D.P., Carr, R.H., Wright, I.P., Pillinger, C. T., 1984. Carbon isotopes in submarine basalts. Earth and Planetary Science Letters, 70(2), 196-206.

McConville, P., Reynolds, J. H., Epstein, S., Roedder, E., 1991. Implanted ^{3}He, ^{4}He, and Xe in further studies of diamonds from Western Australia. Geochimica et Cosmochimica Acta 55, 1977-1989.

Meyer, H.O.A., 1987. Inclusions in diamond. In Mantle xenoliths, Edited by: Nixon, P. H., 501–523.

Navon, O., 1999. Diamond formation in the Earth's mantle. In: Gurney, J.J., Gurney, J.L., Pascoe, M.D., Richardson, S.H. (eds) The J.B. Dawson Volume, Proceedings of the VIIth International Kimberlite Conference. Red Roof Design, Capetown, 584–604.

Nimis, P., Taylor, W.R., 2000. Single-clinopyroxene thermobarometry for garnet peridotites. Part I. Calibration and testing of a Cr-in-Cpx barometer and an enstatite-in-Cpx thermometer. Contributions to Mineralogy and Petrology 139, 541–554.

Ozima, M., Zashu, S., 1983. Primitive helium in diamonds. Science 219(4588), 1067-1068.

Ozima, M., Zashu, S., DP, M., 1985. Helium, argon and carbon isotopic compositions in diamonds and their implications in mantle evolution. Geochemical Journal 19(3), 127-134.

Pearson, D.G., Shirey, S.B., Harris, J.W., Carlson, R.W., 1998. Sulphide inclusions in diamonds from the Koffiefontein kimberlite, S Africa: constraints on diamond ages and mantle Re–Os systematics. Earth and Planetary Science Letters, 160(3-4), 311-326.

Pigeon, R.T., Smith, C.B., Fanning, C.M., 1989. Kimberlite and lamproite emplacement ages in Western Australia. In Ross J. ed. Kimberlites and Related Rocks, Volume 1. Their Composition, Occurrence, Origin and Emplacement, pp. 369-381. Geological Society of Australia Special Publication 14.

Pujol, M., Marty, B., Burgess, R., Turner, G., Philippot, P., 2013. Argon isotopic composition of Archaean atmosphere probes early Earth geodynamics. Nature, 498(7452), 87-90.

Rayner, M.J., Jaques A.L., Boxer, G.L., Smith, C.B., Lorenz, V., Moss, S.W., Webb, K., Ford, D., 2018. The geology of the Argyle (AK1) diamond deposit, Western Australia. Society of Economic Geologists, Special Publication 20, 89–117.

Rege, S., Griffin, W. L., Pearson, N. J., Araújo, D., Zedgenizov, D., O'Reilly, S. Y., 2010. Trace-element patterns of fibrous and monocrystalline diamonds: Insights into mantle fluids. Lithos 118(3-4), 313-337.

Richardson, S.H., 1986. Latter-day origin of diamonds of eclogitic paragenesis. Nature 322, 623-626.

Rudnick, R.L., Gao, S., 2014. Composition of the continental crust. In: Treatise on geochemistry. Elsevier, Amsterdam 3, 1-51.

Sarda, P., Staudacher, T., Allègre, C.J., 1988. Neon isotopes in submarine basalts. Earth and Planetary Science Letters 91(1-2), 73-88.

Schulze, D.J., Harte, B., Edinburgh Ion Microprobe Facility staff, Page, F.Z., Valley, J.W., Channer, D. M.D., Jaques, A.L., 2013. Anticorrelation between low $\delta^{13}C$ of eclogitic diamonds and high $\delta^{18}O$ of their coesite and garnet inclusions requires a subduction origin. Geology 41(4), 455-458.

Seta, A., Matsumoto, T., Matsuda, J.I., 2001. Concurrent evolution of $^{3}He/^{4}He$ ratio in the Earth's mantle reservoirs for the first 2 Ga. Earth and Planetary Science Letters 188, 211-219.

Shelkov, D.A., Verchovsky, A.B., Milledge, H.J., Pillinger, C.T., 1998. The radial distribution of implanted and trapped 4He in single diamond crystals and implications for the origin of carbonado. Chemical Geology 149(1-2), 109-116.

Smart, K.A., Chacko, T., Stachel, T., Muehlenbachs, K., Stern, R.A., Heaman, L.M., 2011. Diamond growth from oxidized carbon sources beneath the Northern Slave Craton, Canada: a $\delta^{13}C$–N study of eclogite-hosted diamonds from the Jericho kimberlite. Geochimica et Cosmochimica Acta 75(20), 6027-6047.

Smye, A.J., Jackson, C.R., Konrad-Schmolke, M., Hesse, M.A., Parman, S.W., Shuster, D.L., Ballentine, C.J., 2017. Noble gases recycled into the mantle through cold subduction zones. Earth and Planetary Science Letters 471, 65-73.

Speich, L., Kohn, S.C., Bulanova, G.P., Smith, C.B., 2018. The behaviour of platelets in natural diamonds and the development of a new mantle thermometer. Contributions to Mineralogy and Petrology 173(5), 39.

Stachel, T., Harris, J.W., Hunt, L., Muehlenbachs, K., Kobussen, A.F., and Edinburgh Ion Micro-Probe Facility., 2018. Argyle diamonds: How subduction along the Kimberley craton edge generated the world's biggest diamond deposit. Society of Economic Geologists, Special Publication 20, 145–167.

Staudacher, T., Allègre, C.J., 1988. Recycling of oceanic crust and sediments: the noble gas subduction barrier. Earth and Planetary Science Letters, 89(2), 173-183.

Staudacher, T., Sarda, P., Richardson, S. H., Allègre, C. J., Sagna, I., Dmitriev, L.V., 1989. Noble gases in basalt glasses from a Mid-Atlantic Ridge topographic high at 14 N: geodynamic consequences. Earth and Planetary Science Letters, 96(1-2), 119-133.

Stern, R.A. Palot, M., Howell, D., Stachel, T., Pearson, D.G., Cartigny, P., Oh, A., 2014. Methods and reference materials for SIMS diamond C-and N-isotope analysis. Canadian Centre for Isotopic Microanalysis (CCIM), Research Report 14–01, University of Alberta, Education and Research Archive.

Taylor, W.R., Jaques, A.L., Ridd, M., 1990. Nitrogen-defect aggregation characteristics of some Australasian diamonds: Time-temperature constraints on the source regions of pipe and alluvial diamonds. American Mineralogist 75, 1290-1310.

Taylor, W.R., Canil, D., Milledge, H.J., 1996. Kinetics of Ib to IaA nitrogen aggregation in diamond. Geochimica et Cosmochimica Acta 60(23), 4725-4733.

Timmerman, S., Koornneef, J.M., Chinn, I.L., Davies, G.R., 2017. Dated eclogitic diamond growth zones reveal variable recycling of crustal carbon through time. Earth and Planetary Science Letters, 463, 178-188.

Timmerman, S., Honda, M., Phillips, D., Jaques, A.L., Harris, J.W., 2018. Noble gas geochemistry of fluid inclusions in South African diamonds: implications for the origin of diamond-forming fluids. Mineralogy and Petrology, 112(1), 181-195.

Timmerman, S., Krebs, M.Y., Pearson, D.G., Honda, M., 2019. Diamond-forming media through time – trace element and noble gas systematics of diamonds formed over 3 billion years of Earth's history. Geochimica et Cosmochimica Acta 257, 266-283.

Tolstikhin, I.N., Verchovsky, A.B., Kamensky, I.L., Skiba, V.I., Gannibal, M.A., Vetrin, V.R., Tarakanov, S.V., 2016. Amphibole: A major carrier of helium isotopes in crustal rocks. Chemical Geology 444, 187-198.

Trautman, R.L., 1999. The nature and genesis of microdiamonds. University of Western Australia.

Tucker, J.M., Mukhopadhyay, S., 2014. Evidence for multiple magma ocean outgassing and atmospheric loss episodes from mantle noble gases. Earth and Planetary Science Letters 393, 254-265.

Tyler, I.M., Hocking, R.M., Haines, P.W., 2012. Geological evolution of the Kimberley region of Western Australia. Episodes 35(1), 298-306.

Viljoen, K., 2002. An infrared investigation of inclusion-bearing diamonds from the Venetia kimberlite, Northern Province, South Africa: implications for diamonds from craton-margin settings. Contributions to Mineralogy and Petrology 144, 98-108.

Wada, N., Matsuda, J.I., 1998. A noble gas study of cubic diamonds from Zaire: constraints on their mantle source. Geochimica et Cosmochimica Acta 62(13), 2335-2345.

White, W.M, Klein, E.M., 2014. Composition of the oceanic crust. In: Treatise on geochemistry. Elsevier, Amsterdam 4, 457-496.

Wiggers de Vries, D. , Pearson, D.G., Bulanova, G.P., Smelov, A.P., Pavlushin, A.D., Davies, G.R., 2013. Re–Os dating of sulphide inclusions zonally distributed in single Yakutian diamonds: Evidence for multiple episodes of Proterozoic formation and protracted timescales of diamond growth. Geochimica et Cosmochimica Acta, 120, 363-394.

Yatsevich, I., Honda, M., 1997. Production of nucleogenic neon in the Earth from natural radioactive decay. Journal of Geophysical Research: Solid Earth 102(B5), 10291-10298.

Zhang, X., Honda, M., Hamilton, D., 2016. Performance of the high resolution, multi-collector helix mc plus noble gas mass spectrometer at the Australian National University. Journal of The American Society for Mass Spectrometry 27(12), 1937-1943.

Zhang, X., Honda, M., 2017. Minimisation of pressure dependent mass discrimination in the ion source of the Helix MC Plus noble gas mass spectrometer. Chemical Geology 473, 50-54.

Figures captions

Figure 1 Cathodoluminescence images of the diamonds with FTIR spot analyses (white squares; transect A-B) and SHRIMP spot analyses (yellow circles; transect starting at 1) indicated. For visibility the SHRIMP spots are presented larger than the actual spot size of 27 µm.

Figure 2 Nitrogen content and aggregation state of studied Argyle diamonds. Isotherms calculated based on 2.0 Gyr (a; solid lines) and 0.4 Gyr (a; dashed lines) residence times for peridotitic and 0.4 Gyr (b, c) for eclogitic diamonds respectively (see text). Where no paragenesis was known, a residence time of 0.4 Gyr was assumed as most diamonds are likely eclogitic based on their carbon isotope compositions.

Figure 3 Helium isotope data of the studied Argyle diamonds versus ^{3}He (a) and ^{4}He (b) concentrations. Literature data of gem diamonds (in triangle symbols) with known paragenesis (Orapa; Kurz et al., 1987) are given as reference. Fitted linear and hyperbolic lines are provided in green for peridotitic diamonds and hyperbolic lines in purple and red for eclogitic diamonds. Solid lines show radiogenic ingrowth models and the dashed line for mixing between slab and mantle. See text for details. c) importance of radiogenic ingrowth to the R/Ra value, d) R/Ra values versus the reciprocal of the helium concentration, including radiogenic ingrowth and mixing lines (see discussion for details).

Figure 4 Neon isotope composition of sample A50-1 relative to the air-solar and air-MORB mixing lines.

Figure 5 R/Ra versus carbon isotope composition in Argyle diamonds. Diamond A17-1 is excluded because of suspected addition of cosmogenic ^{3}He. Crosses for fibrous diamonds from various locations (Burgess et al., 1998; 2009), white diamonds for potential eclogitic diamonds from Argyle (Honda et al., 2012), orange diamonds for eclogitic diamonds from southern Africa (Timmerman et al., 2019), green squares for peridotitic, purple diamonds for eclogitic samples of this study. Mixing lines and mixing+radiogenic ^{4}He ingrowth (over 1600 Myr with various U contents) lines are calculated between a mantle component at 1600 Ma (26.6 R/Ra without radiogenic ingrowth and -5‰; Seta et al., 2001; Cartigny, 2005) and a subduction component (0.005 R/Ra and 0 to -27‰ for oceanic crust, set at -25‰; Ballentine and Burnard, 2002; Li et al., 2019). For reference MORB (Graham, 2002; Mattey et al,. 1984) and SCLM values (Day et al., 2005; Cartigny, 2005) are shown. The r values indicate the $He/C_{subduction}$: He/C_{mantle} ratio.

Figure 6 a) Frequency distribution of R/Ra values of eclogitic and peridotitic diamonds. Previously published data for Argyle diamonds from Honda et al. (2012) and Orapa diamonds from Kurz et al. (1987). b) Helium versus $^{4}He/^{40}Ar$ compositions. Symbols are the same as in figure 5. Inset shows data plotted on a logarithmic scale, with MORB as a reference (Graham, 2002; Staudacher et al., 1989).

Figure 7 R/Ra values (a) and $^{40}Ar/^{4}He$ ratios (measured $^{40}Ar/^{4}He$ are upper limits of $^{40}Ar^{*}/^{4}He$ ratios) (b) coupled to the mantle residence temperatures of eclogitic (in purple) and peridotitic (in green) Argyle diamonds. Fields for SCLM, MORB, and subducted material are shown (Staudacher et al., 1989; Day et al., 2005; Ballentine and Burnard, 2002). c) Mantle residence temperatures from N aggregation and carbon isotope compositions, including previously published data (Jaques et al., 1989a; Stachel et al., 2018). d) Schematic section across the eastern margin of the Kimberley Craton and Halls Creek Orogen showing accreted subducted crust at the base of the SCLM (blue), the migration of subducted fluids into the SCLM, and diamond formation.

Figure 8 Depth profile with colour intensities expressing the percentage of subduction influence linearly (using 0.005 R/Ra for subduction and 6 R/Ra for SCLM as end-members). Argyle paleogeotherm (modified after Jaques et al., 2018) based on P-T estimates for mantle Cr-diopsides (Nimis and Taylor, 2000) from the Argyle pipe and the FITPLOT routine of Mather et al. (2011). The graphite – diamond transition is from Kennedy and Kennedy (1976).

Table 1 Overview of the studied diamonds from Argyle. The minimum and maximum of the carbon isotope composition, nitrogen content, aggregation state and temperature are given. Individual analyses of core-rim traverses can be found in the appendix.

Sample	Colour	Inclusions	Paragenesis	min $\delta^{13}C$ (‰)	max $\delta^{13}C$ (‰)	N (at ppm)	%B
A50	col-light grey	-	E?	-12.3	-11.5	20-30	46-88
A51	col-light grey	alt E-grt	E	-16.6	-14.0	15-49	82-100
A52	col-light grey	cs	E	-10.9	-10.0	53-112	99-100
A53	col-light grey	-	E?	-11.6	-8.9	22-145	93-100
A54	brown	3 E-grt	E	-13.4	-11.5	65-163	78-91
A55	col-light grey	-	E?	-12.4	-8.6	38-97	100
A56	light brown	-	-	-9.1	-6.7	84-279	78-95
A57	col-light grey	-	-	-10.8	-8.6	50-209	84-96
A58	light brown	-	E?	-13.1	-9.2	90-145	80-89
A59	brown	2 E-grt	E	-12.0	-8.6	57-338	84-94
A60	light brown	4 E-grt, 1 E-cpx	E	-9.3	-8.3	104-489	58-93
A17	colourless	4 E-grt	E	-11.2	-9.7	80-107	73-75
Arg-43	brown	3 E-cpx	E	-9.2	-8.1	64-888	65-98
Arg-42	brown	E-cpx	E	-11.1	-7.8	67-348	69-95
Arg-36	brown	cs	E	-10.7	-8.5	91-322	84-97
Arg-26	brown	cs	E	-10.5	-9.4	67-97	73-80
A2-010	colourless	cs	E	-6.9	-4.7	112-286	79-93
Arg-006	brown	2 ol	P	-7.7	-6.3	30-419	65-100
Arg-41	brown	ol	P	-4.4	-4.0	107-680	15-49
Arg-89	brown	1 ol, 1 grp	P	-7.8	-7.2	154-400	76-91

* col = colourless

** Nitrogen aggregation temperature based on 0.4 Ga residence for E-type and unknown paragenesis and 2 Ga for P-type. At 100% B aggregation state no temperatures can be calculated and it is assumed the residence temperature was ≥1350°C.

*** 1) Bulanova et al. 2018; 2) Kohn et al. 2016

**** a = Raman, b = FTIR, c = CL, d = EPMA

Table 2 Major element compositions of mineral inclusions of Argyle diamonds.

Sample	A54	A54	A59	A60	A17	A17	Arg-006	Arg-89
Mineral	grt 1	grt 2	grt	grt 1	grt 1	grt 2	ol	ol
P_2O_5	na	na	0.31	0.10	0.25	0.14	na	na
SiO_2	40.11	40.26	39.87	41.94	41.34	40.87	40.85	42.21
TiO_2	0.86	0.91	1.18	0.57	0.26	0.56	<0.03	<0.03
Al_2O_3	21.97	22.06	19.98	22.94	22.48	22.30	0.09	<0.02
Cr_2O_3	0.06	0.05	0.04	0.10	0.05	0.05	0.14	0.19
FeO	18.73	18.59	17.42	10.78	10.76	11.71	7.86	6.53
NiO	<0.03	<0.03	<0.03	<0.03	<0.03	0.04	0.41	0.36
MnO	0.31	0.31	0.32	0.24	0.18	0.21	0.10	0.08
MgO	9.44	9.45	8.29	14.13	11.69	11.68	50.75	51.00
CaO	9.20	9.01	11.48	9.89	13.08	12.15	0.04	0.02
Na_2O	0.42	0.44	0.54	0.22	0.29	0.29	<0.03	<0.03
K_2O	<0.03	<0.03	0.03	0.04	0.04	0.04	<0.03	<0.03
Total	101.11	101.09	99.47	100.94	100.43	100.03	100.28	100.41
Cations (apfu 12O)	8.02	8.01	8.03	7.99	8.01	8.01	3.01	2.98
Mg#	47.3	47.5	45.9	70.0	65.9	64.0	92.0	93.3

*na = not available

**grt = garnet, ol = olivine

*** detection limits are ~250-300 ppm for TiO_2, K_2O, NiO, ~200 ppm for Na_2O and ~100 ppm for Al_2O_3.

Table 3 He and Ar concentrations and isotopic compositions of Argyle diamonds.

Sample	Comment	Paragenesis	weight (g)	^{4}He (cc/g)	1SD	^{3}He (cc/g)	1SD	^{3}He/^{4}H
A50-1	rim	E?	0.03870	2.22E-06	1.16E-08	1.93E-13	3.02E-14	8.69E-
A50-2	core	E?	0.05575	4.83E-06	2.56E-08	3.86E-13	3.83E-14	7.98E-
A51-2	int	E	0.04221	2.79E-06	1.46E-08	5.17E-13	4.26E-14	1.85E-
A52	whole	E	0.03682	9.11E-07	4.79E-09	5.43E-13	3.98E-14	5.96E-
A54-1	core	E	0.02601	1.83E-07	1.05E-09	6.23E-13	8.19E-14	3.40E-
A54-2	rim	E	0.02828	2.00E-06	1.04E-08	5.80E-13	7.54E-14	2.91E-
A59-1	core	E	0.01811	2.19E-07	1.36E-09	blb	-	<1.01E
A60-3	rim	E	0.02413	2.88E-06	1.50E-08	blb	-	<7.75E
A17-1	int	E	0.03273	1.61E-07	9.15E-10	5.34E-12	1.29E-13	3.31E-
A81-2	int	E	0.00643	9.87E-07	5.43E-09	2.11E-12	1.94E-13	2.14E-
Arg006-1	core	P	0.01118	6.06E-06	3.17E-08	2.48E-12	1.65E-13	4.09E-
Arg006-2	rim	P	0.00318	2.58E-06	1.43E-08	6.61E-12	5.04E-13	2.56E-
Arg41-1	core	P	0.00837	2.19E-06	1.15E-08	3.32E-12	2.68E-13	1.52E-
Arg41-23	rim	P	0.00760	2.48E-07	2.27E-09	1.09E-12	2.44E-13	4.39E-
Arg89-2	rim	P	0.00578	5.31E-06	2.80E-08	3.99E-12	2.01E-13	7.51E-

blb = below blank

Table 3 continued

Sample	Paragenesis	^{40}Ar (cc/g)	1SD	$^{40}Ar/^{36}Ar$	1SD	$^{38}Ar/^{36}Ar$	1SD	$^{4}He/^{40}Ar$	1SD
A50-1	E?	blb	-	-	-	-	-	-	-
A50-2	E?	7.17E-08	5.69E-10	552	7	0.175	0.003	67.5	1.1
A51-2	E	8.41E-08	6.67E-10	775	12	0.18	0.004	33.2	0.6
A52	E	blb	-	-	-	-	-	-	-
A54-1	E	blb	-	-	-	-	-	-	-
A54-2	E	1.26E-08	1.22E-10	247	5	0.186	0.01	158.7	3.2
A59-1	E	2.23E-08	1.84E-10	344	9	0.177	0.012	9.8	0.2
A60-3	E	2.92E-08	2.42E-10	260	4	0.16	0.005	98.4	1.7
A17-1	E	blb	-	-	-	-	-	-	-
A81-2	E	blb	-	-	-	-	-	-	-
Arg006-1	P	1.70E-07	1.35E-09	556	10	0.185	0.005	35.7	0.6
Arg006-2	P	blb	-	-	-	-	-	-	-
Arg41-1	P	1.22E-07	9.85E-10	6033	1101	0.196	0.089	17.9	0.3
Arg41-23	P	7.94E-08	6.64E-10	261	5	0.178	0.006	3.1	0.1
Arg89-2	P	1.13E-06	8.98E-09	299	3	0.186	0.002	4.7	0.1

Highlights

- Difference in He-Ar compositions between eclogitic and peridotitic diamonds
- Low $\delta^{13}C$ values coupled to low $^{3}He/^{4}He$ ratios in eclogitic Argyle diamonds
- $^{3}He/^{4}He$ ratio of peridotitic diamonds is lower than typical lithospheric mantle
- Noble gas subduction signature at 205-180 km and fluid migration to ~165 km depth

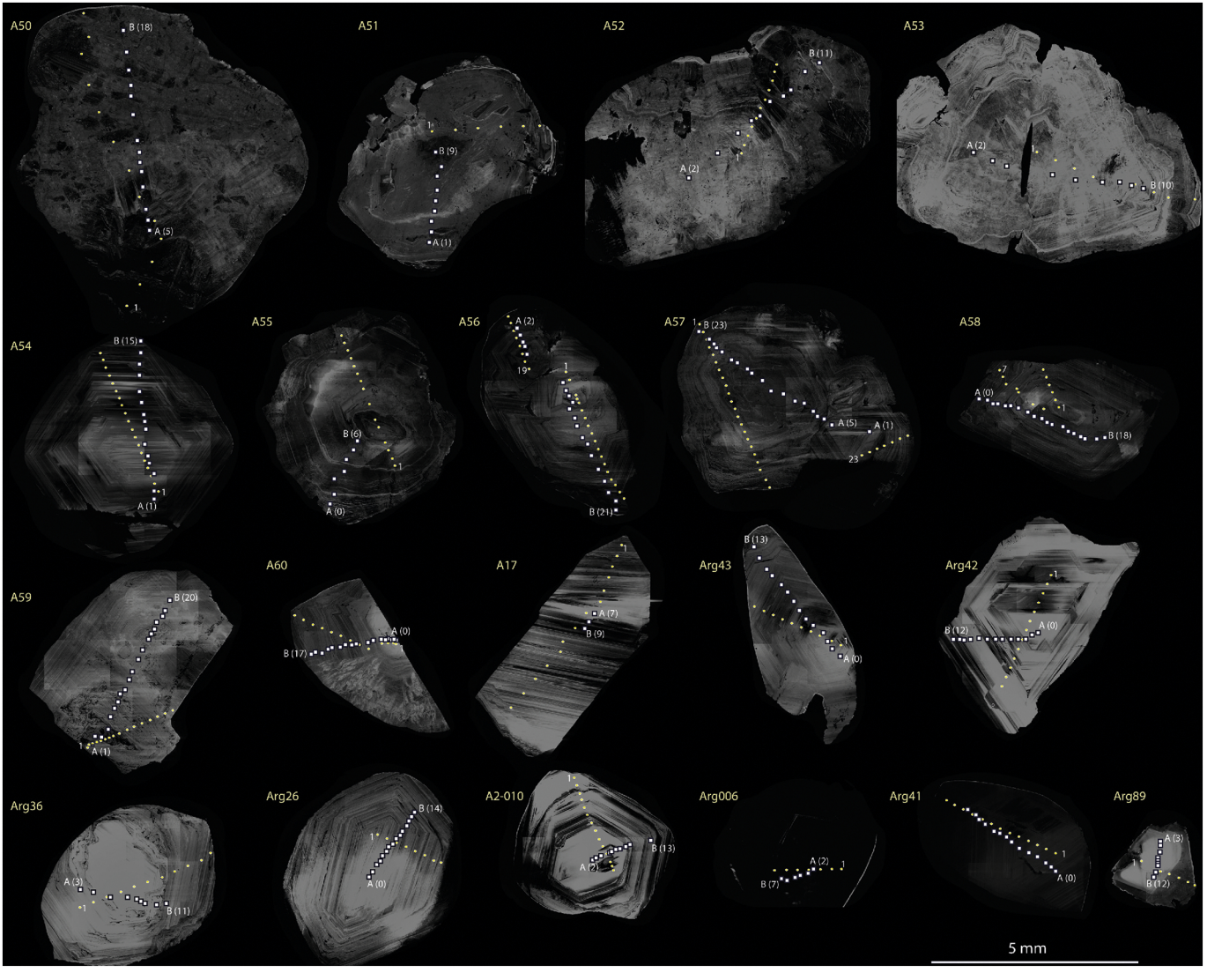
A50
B (18)
A (5)
1
A51
1
B (9)
A (1)
A52
B (11)
A (2)
1
A53
A (2)
1
B (10)
A54
B (15)
1
A (1)
A55
B (6)
1
A (0)
A56
A (2)
19
1
B (21)
A57
1
B (23)
A (5)
A (1)
23
A58
7
A (0)
1
B (18)
A59
B (20)
1
A (1)
A60
A (0)
B (17)
A17
1
A (7)
B (9)
Arg43
B (13)
1
A (0)
Arg42
1
B (12)
A (0)
Arg36
A (3)
1
B (11)
Arg26
B (14)
1
A (0)
A2-010
1
A (2)
B (13)
Arg006
A (2)
1
B (7)
Arg41
1
A (0)
Arg89
A (3)
1
B (12)
5 mm

Figure 1

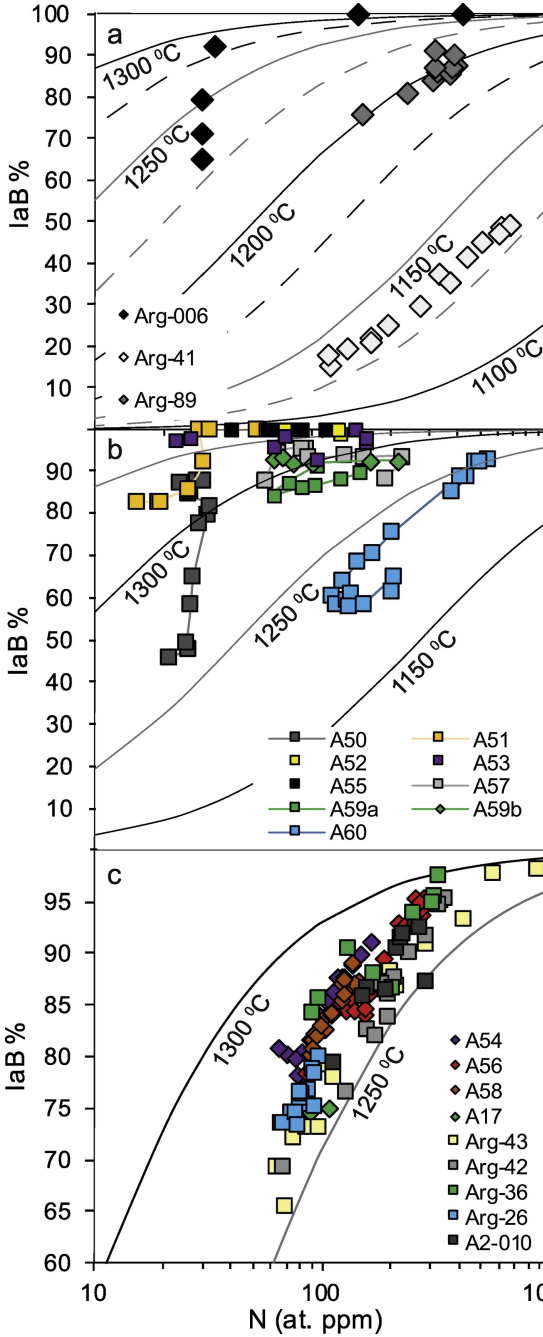
a
b
c
IaB %
N (at. ppm)
1300 °C
1250 °C
1200 °C
1150 °C
1100 °C
Arg-006
Arg-41
Arg-89
A50
A51
A52
A53
A55
A57
A59a
A59b
A60
A54
A56
A58
A17
Arg-43
Arg-42
Arg-36
Arg-26
A2-010

Figure 2

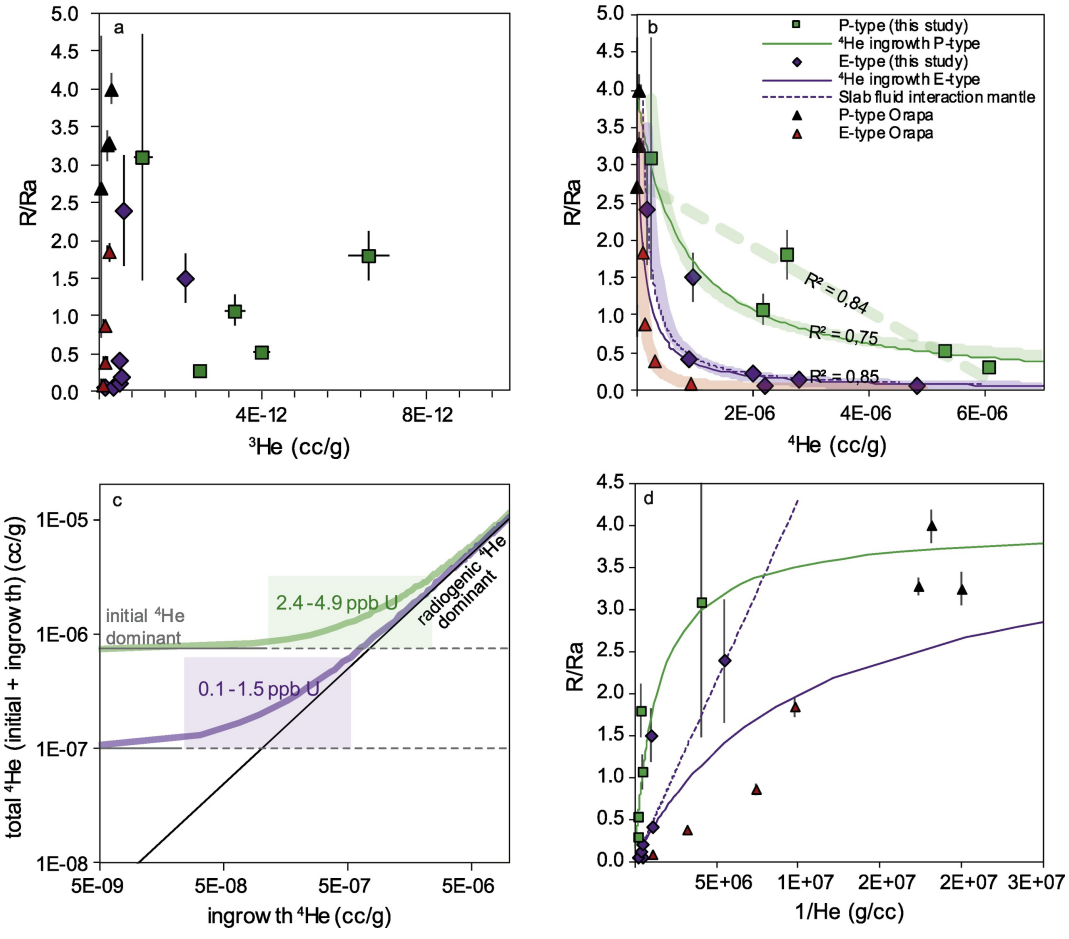
a
R/Ra
^{3}He (cc/g)
b
P-type (this study)
^{4}He ingrowth P-type
E-type (this study)
^{4}He ingrowth E-type
Slab fluid interaction mantle
P-type Orapa
E-type Orapa
R² = 0,84
R² = 0,75
R² = 0,85
^{4}He (cc/g)
c
initial ^{4}He dominant
2.4 - 4.9 ppb U
0.1 - 1.5 ppb U
radiogenic ^{4}He dominant
total ^{4}He (initial + ingrowth) (cc/g)
ingrowth ^{4}He (cc/g)
d
R/Ra
1/He (g/cc)

Figure 3

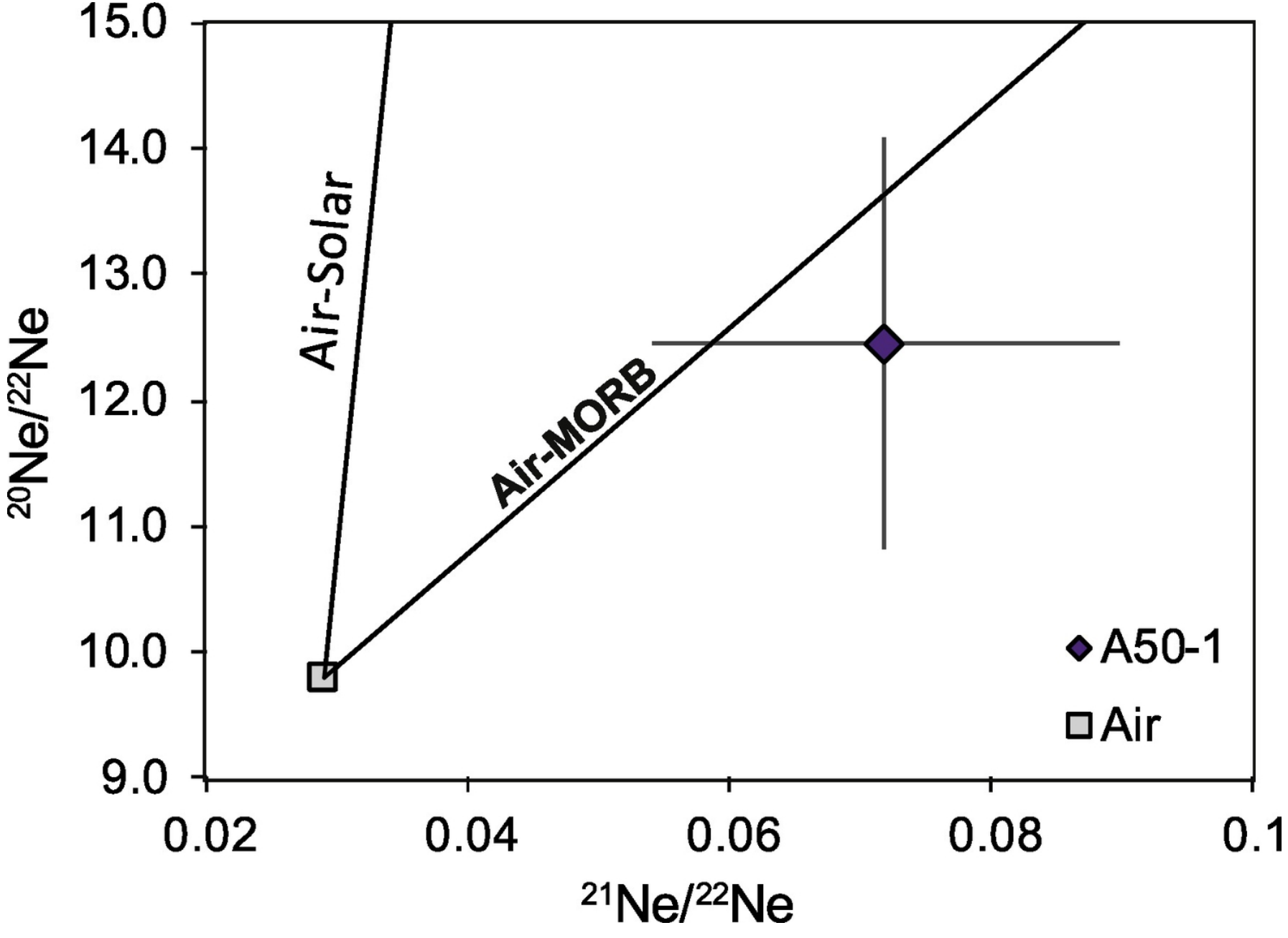
15.0
14.0
13.0
12.0
11.0
10.0
9.0
$^{20}Ne/^{22}Ne$
0.02
0.04
0.06
0.08
0.1
$^{21}Ne/^{22}Ne$
Air-Solar
Air-MORB
A50-1
Air

Figure 4

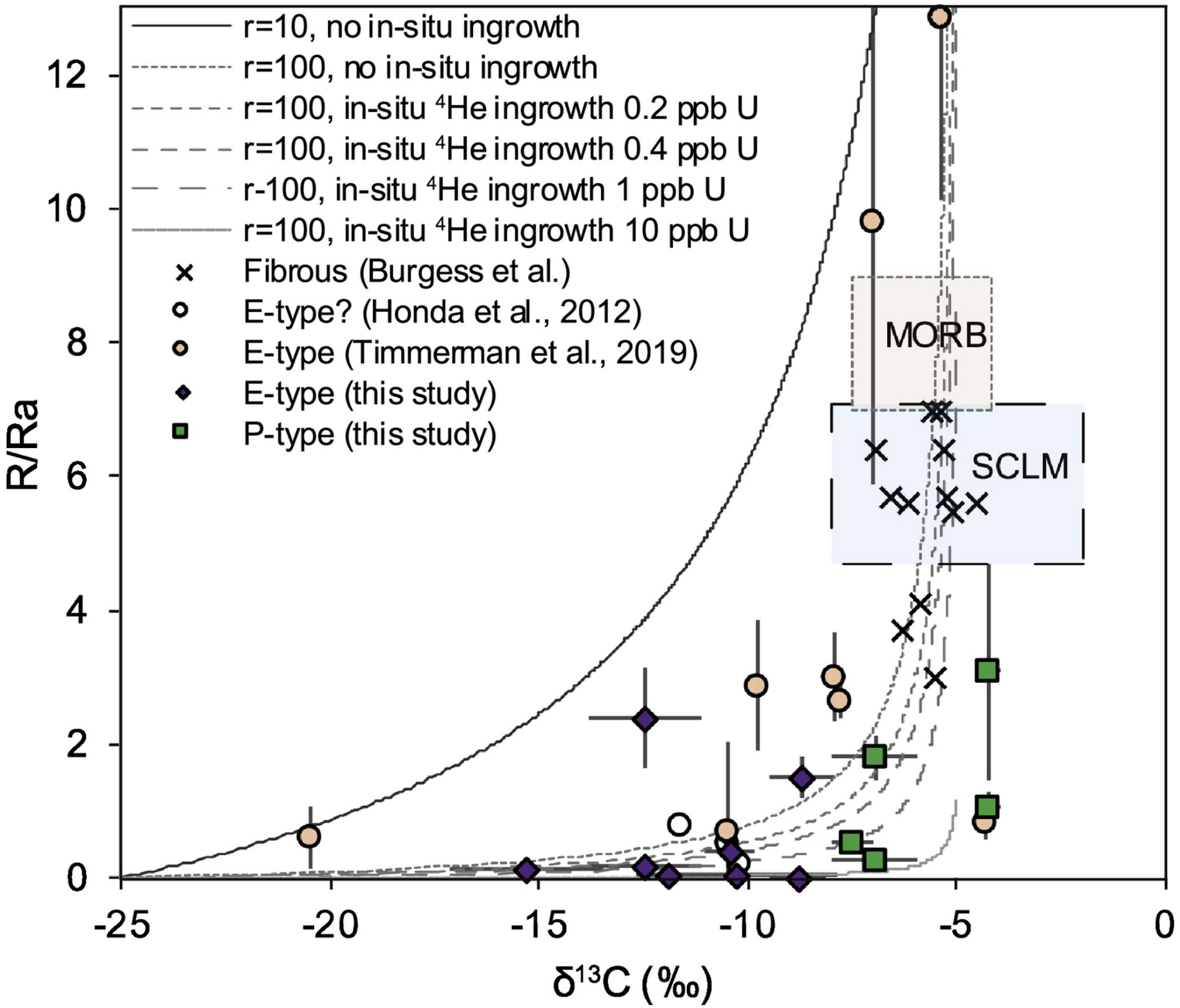
r=10, no in-situ ingrowth
r=100, no in-situ ingrowth
r=100, in-situ 4He ingrowth 0.2 ppb U
r=100, in-situ 4He ingrowth 0.4 ppb U
r-100, in-situ 4He ingrowth 1 ppb U
r=100, in-situ 4He ingrowth 10 ppb U
Fibrous (Burgess et al.)
E-type? (Honda et al., 2012)
E-type (Timmerman et al., 2019)
E-type (this study)
P-type (this study)
MORB
SCLM
R/Ra
δ13C (‰)
0
2
4
6
8
10
12
-25
-20
-15
-10
-5
0

Figure 5

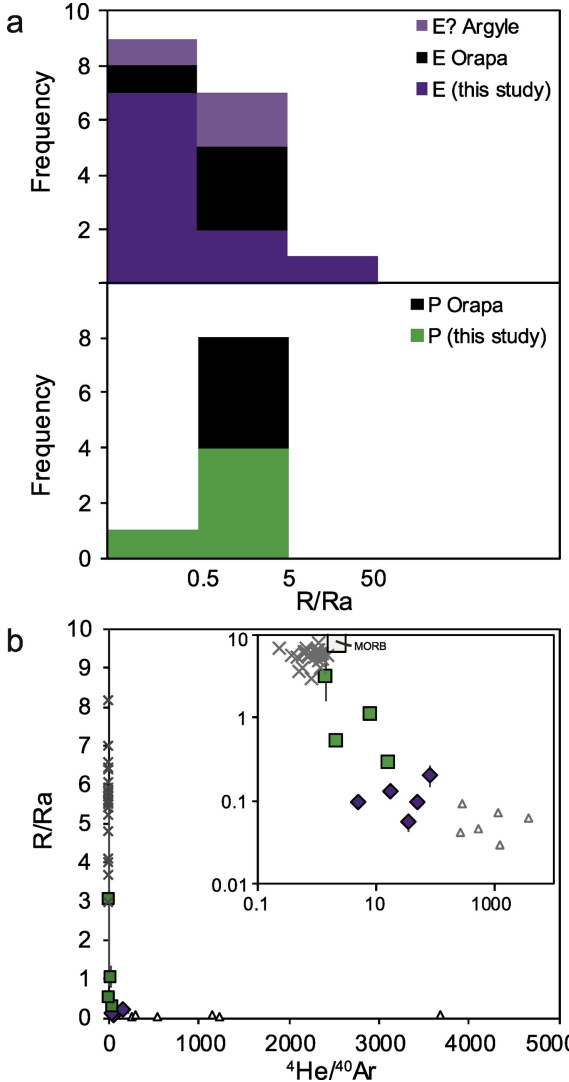
a
E? Argyle
E Orapa
E (this study)
Frequency
P Orapa
P (this study)
Frequency
0.5
5
50
R/Ra
b
MORB
R/Ra
0.01
0.1
1
10
0.1
10
1000
0
1000
2000
3000
4000
5000
4He/40Ar

Figure 6

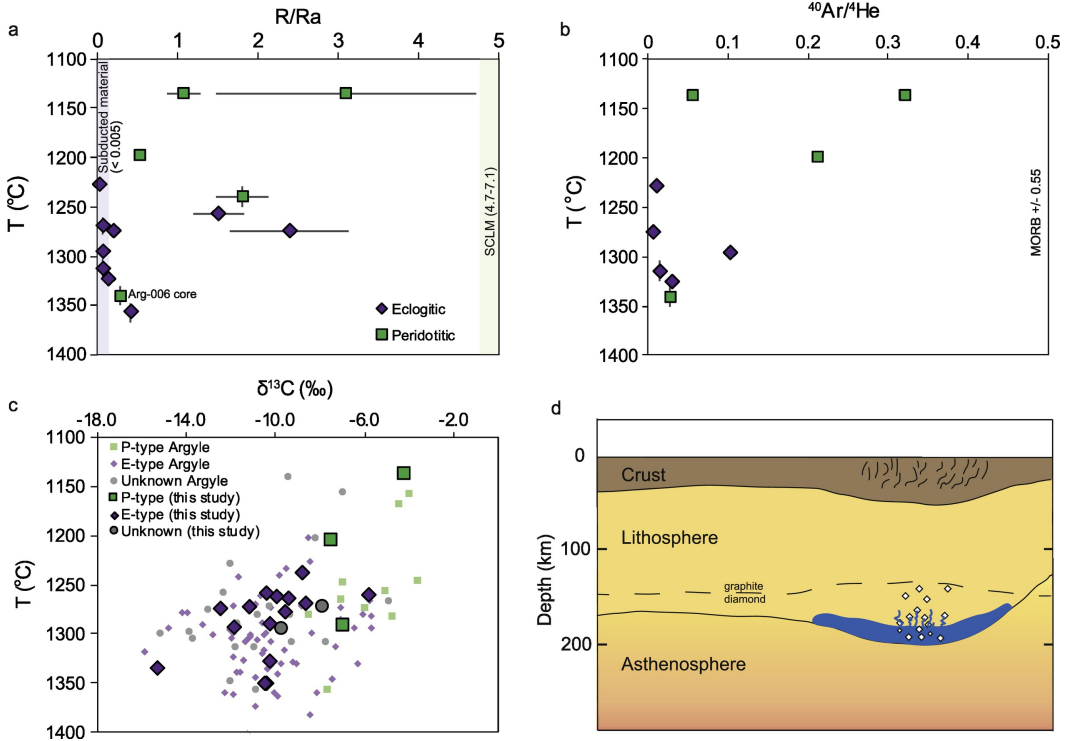
a
R/Ra
0
1
2
3
4
5
T (°C)
1100
1150
1200
1250
1300
1350
1400
Subducted material (< 0.005)
SCLM (4.7-7.1)
Arg-006 core
Eclogitic
Peridotitic
b
40Ar/4He
0
0.1
0.2
0.3
0.4
0.5
T (°C)
MORB +/- 0.55
c
δ13C (‰)
-18.0
-14.0
-10.0
-6.0
-2.0
T (°C)
P-type Argyle
E-type Argyle
Unknown Argyle
P-type (this study)
E-type (this study)
Unknown (this study)
d
0
100
200
Depth (km)
Crust
Lithosphere
graphite
diamond
Asthenosphere

Figure 7

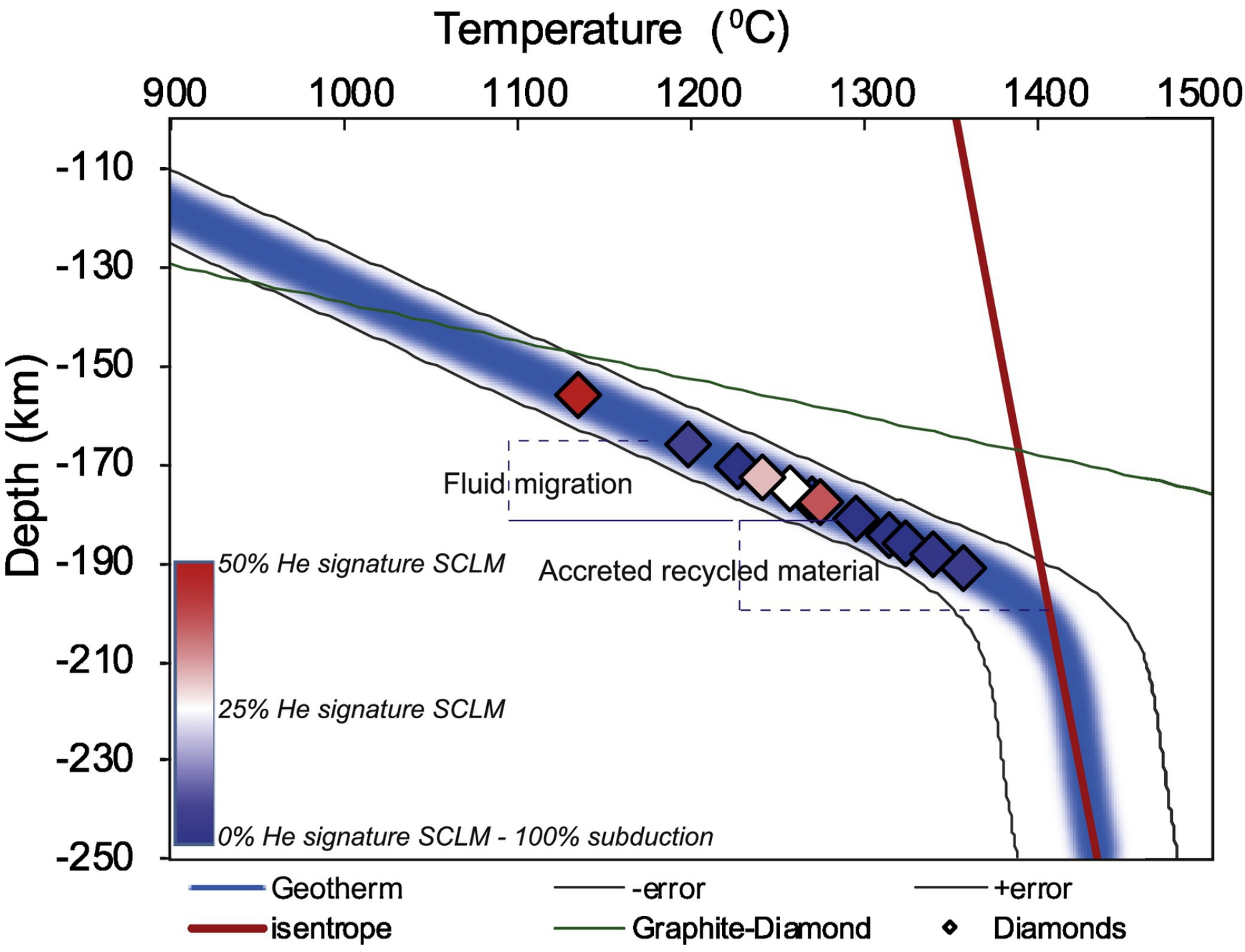
Temperature (⁰C)
900
1000
1100
1200
1300
1400
1500
-110
-130
-150
-170
-190
-210
-230
-250
Depth (km)
Fluid migration
Accreted recycled material
50% He signature SCLM
25% He signature SCLM
0% He signature SCLM - 100% subduction
Geotherm
-error
+error
isentrope
Graphite-Diamond
Diamonds

Figure 8